6th BSME International Conference on Thermal Engineering (ICTE 2014)

Design and analysis of feedstock mixing mechanism for micro metal injection moulding

A. A. Abdullahi, I. A. Choudhury[*], A. Hossain, M. Azuddin

Manufacturing Systems Integration, Department of Mechanical Engineering, University of Malaya, 50603 Kuala Lumpur, Malaysia

Abstract

The need for homogeneous metal powder and binder mixing is paramount in injection moulding process as it affect product quality significantly. However available commercial feedstocks may not be suitable especially for production of micro parts with high aspect ratio. Therefore, this research proposes a new mixer design that incorporate mixing and granulation of the feedstock for components production at micro level. Also metal powder/ binder flow in the mixing chamber is investigated. The design specifications and simulation were based on powder loading, powder size and shape, binder formulation, sequence of material addition, mixing time, temperature and shear rate with finite element analysis. The simulation results show a favourable and visible design anticipation of the mixing mechanism and mixed feedstock. Conclusively development of this design will enhance micro metal moulding productivity and improve production cycle time.
© 2015 The Authors. Published by Elsevier Ltd.
Peer-review under responsibility of organizing committee of the 6th BSME International Conference on Thermal Engineering (ICTE 2014).

Keywords: feedstock; design; mixing mechanism; micro parts; micro metal; injection moulding; flow analysis

1. Introduction

Industrial production of product begin from selection and preparation of raw material to be used for the manufacture of the finished product. This usually includes adoption of manufacturing techniques and procedure which are exclusively unique for different product development. Therefore, mixing of the constituent element or components in

----

* Corresponding author. Tel.: +60163704658; fax: +60379675317.
  E-mail address: imtiaz@um.edu.my

Nomenclature

ρ	density
$\dot{\gamma}$	effective shear rate
$\underline{D}$	rate of deformation tensor
β	a constant parameter with units of time
η_∞	infinite shear viscosity
λ	mixing index
δ	screw tip-barrel wall clearance
τ	shear tensor
η	shear viscosity
α	temperature coefficient of viscosity
η_0	zero shear viscosity
a	width of transition region
C(T)	heat capacity
D	barrel diameter
D_A	screw external diameter
D_k	screw core diameter
H	a step function
L	centreline distance
n	dimensionless constant
P	pressure
q	heat flux
r	volumetric heat source
s	screw-screw clearance (s)
t	time
T	temperature
T_0	barrel surface temperature
T_s	screw pitch
V	velocity
z	number of threads

production processing of Pharmaceutical, Chemical, Cement, Food, and Powder Injection Moulding (PIM) products have to achieve efficient and homogenous mixing.

However, homogeneous blending of the constituent elements has been the problem. Even though, investigation of particle mixing mechanisms has received fundamental attention since 1954 by Lancy's study, as cited in [1]. In general, mixing mechanism of particles were classified into three categories. These are convection, diffusion and shearing mechanisms of mixing. Meanwhile mixers combine these mechanisms to achieve optimum processing condition [1, 2]. But their performance has been hindered by design and process conditions [3, 4]. Hence, there is a need for optimizing design parameters as well as process conditions. This is for the fact that preparation of homogenous feedstock greatly influences the product quality of micro metal injection moulding.

In recent time numerical simulation and experimental research are ongoing on the suitability of the screw extruders for mixing mechanism [5-12]. Fig. 1 presents broad classification of mixers based on extrusion principle
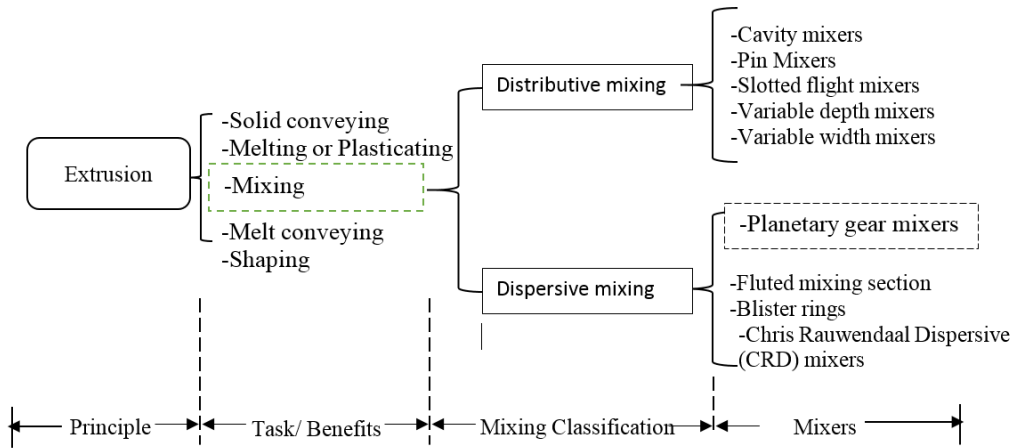
Fig. 1. Mixing mechanism and mixer classification based on plasticising extrusion.

During mixing a typical fluid flow analysis is characterised as either a Newtonian or non-Newtonian fluids. In this study, the fluid within the mixing chamber were considered as non-Newtonian; this fluid exhibits viscoelastic effects.

According to Huang and Kuo [1] computer simulation is a numerical tool that is more cost-effective than carrying out experiments in complex systems. This establishes a basis for design optimisation, scale-up, and control of the system. Nevertheless, there are two common numerical approaches for studying particle mixing: the discrete approach and the continuum approach. Meanwhile, the Monte Carlo Method, Cellular Automata, and Discrete Element Method (DEM) were developed based on discrete approach. In addition, researchers now prefer to analyse granular flow with Computational Fluid Dynamics (CFD), for the fact that continuum approach does not account for system size relative to DEM. Flow pattern of mixing particles can be described as either dispersive or distributive mixing [14-15], as illustrated in Fig. 2.
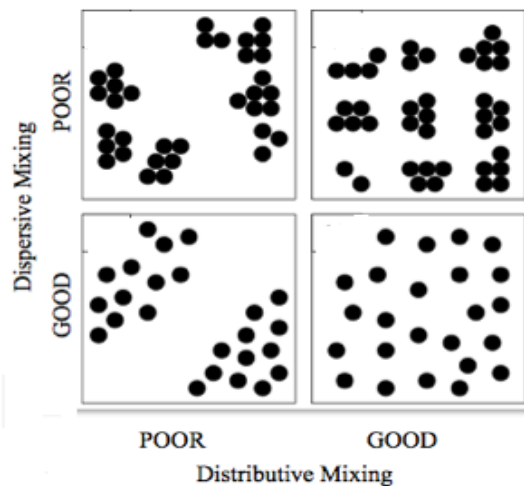
Fig. 2. Dispersive mixing and distributive mixing.

Therefore, the objective of this research is to design a miniature mixer suitable for mixing and granulating of the micro metal injection moulding feedstock constituents, based on extrusion principle. The present research will optimize process conditions of the proposed design using simulation to predict the mixing capabilities of the mixer.

2. Materials and methods

2.1. Schematic of the mixer design

The design analysis and consideration were given to powder size and shape, binder formulation and constitute, sequence of material addition, mixing time and temperature, shear rate and rotor speed.
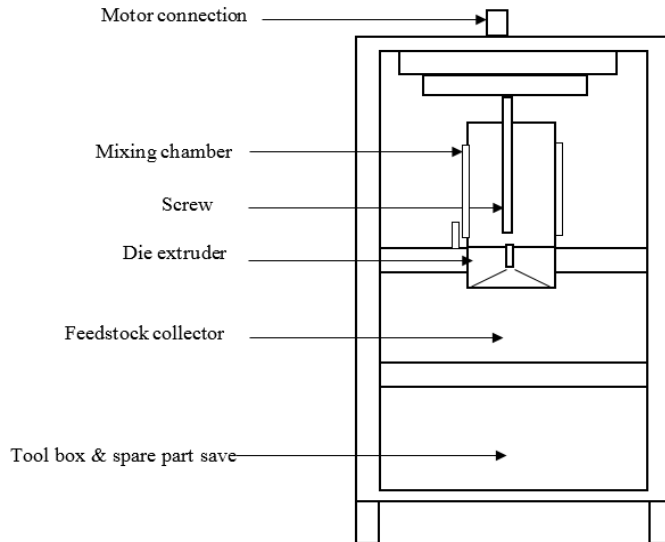
Fig. 3. Schematic of the mixer.

The proposed design shown in Fig. 3 consists of a mixing chamber with screw mixer, a die extruder, and a feedstock collector. The bottom chamber is for keeping tools and spare parts. The design specification for the screw is presented in Table 1.

Table 1: Specification of the double-flighted screw and barrel geometries.

Characteristic variables	Value (mm)
Centreline distance (L)	50
Barrel diameter (D)	61
Screw core diameter (D_k)	38
Screw external diameter (D_A)	60
Screw tip-barrel wall clearance (δ)	0.5
Screw-screw clearance (s)	1
Pitch (T_s)	120
Number of threads (Z)	2

The distance (L) between the screws centre is expressed as:

$$L = \tfrac{1}{2}\left(D_A + D_k\right) + s \tag{1}$$

However, to have proper intermesh between the screws equation (2) must be satisfy [16].

$$\frac{L}{(D_A+s)} \geq \cos\left(\frac{90}{Z}\right) \tag{2}$$

The energy balance of the system involves input from the electric motor and heating elements. However, the heat transfer analysis of the thermal energy supply by the electric heaters to the mixing chamber undergo two forms of the transfer system. At inception the heat transfer is dominated by conduction from the heaters to the barrel and between the barrel to the feedstock in solid state, likewise from feedstock to the screw. Meanwhile, as the feedstock transforms from a solid phase to fluid, a convective transfer sets in at this stage within the mixing chamber. But conduction still remains between the fluid interfaces and the barrel as well as between the screws.

2.2. Mathematical Modelling

The analysis of fluid flow were based finite element method, starting with formulation of the substantive derivative, which account for the motion, displacement and non-isothermal energy conservation of the fluid particle within the mixing chamber. The governing equations of fluid flow are as follows:

$$\nabla . \vec{V} = 0 \tag{3}$$

$$H(v - \vec{V}) + (1 - H)\left[\nabla . \vec{\tau} - \nabla p + \rho\left(\frac{\partial v}{\partial t} + v . \nabla \vec{V}\right)\right] = 0 \tag{4}$$

$$\rho C(T)\left(\frac{\partial T}{\partial t} + v . \nabla T\right) = T . \nabla v + r - \nabla . q \tag{5}$$

Equation (3) is the continuity equation, equation (4) is the momentum and equation (5) is energy equation. The stress tensor and the shear rate is define by equation (6) and equation (7) respectively, in term of the strain rate tensor.

$$\vec{\tau} = 2\eta(\dot{\gamma}, T)\vec{D} \tag{6}$$

$$\dot{\gamma} = \sqrt{2\vec{D} : \vec{D}} \tag{7}$$

In this study, Carreau-Yasuda model is adopted for rheology of the fluid particle and shear viscosity is expressed as:

$$\eta = \eta_\infty + (\eta_0 - \eta_\infty)[1 + (\beta\dot{\gamma})^a]^{\frac{(n-1)}{a}} \tag{8}$$

Since the flow is non-isothermal, then temperature has to be accounted for; by a factor known as the Arrhenius law $H(T)$. The shear viscosity is

$$\eta = \eta_0(\gamma)H(T) \tag{9}$$

The approximate Arrhenius law is expressed as:

$$H(T) = \exp[-\alpha(T - T_0)]$$

(10)

2.3. Simulation

Fluid simulation within the mixing chamber were carried out based on Finite Element Method (FEM), using ANSYS 14.0. This involves five steps namely i) Geometry, ii) Mesh, iii) Setup, iv) Solution, and v) Results

The flow domain of the system is illustrated in Fig. 4, showing the screws and barrel mesh superposition at initial location with 1080 elements and 2302 nodes.
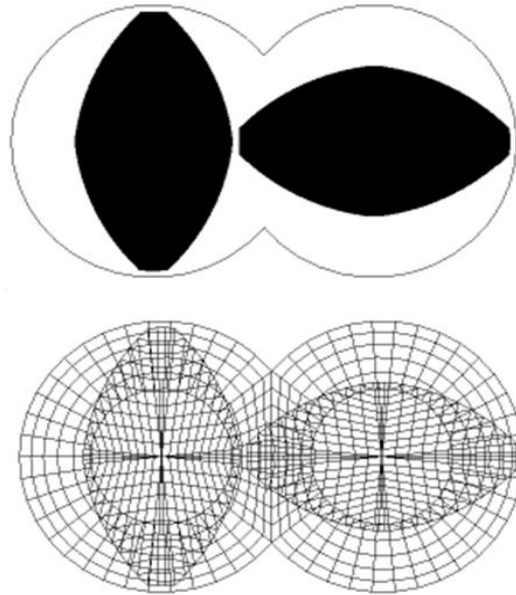
Fig. 4. Flow domain geometry and meshes at the initial position.

This study proposes to mix Aluminum Powder, High Density Polyethylene (HDPE), Paraffin Wax (PW) and Stearic Acid (SA) for the preparation of micro metal injection moulding feedstock. However, to investigate the behaviour of the feedstock; some basic assumptions were made such as the fluid is non-Newtonian and exhibits laminar flow with high viscosity; the flow is non-isothermal, incompressible, and nonslip condition existed at barrel wall and screw flight and the influence of both inertia and gravity effects were neglected. The proprieties of the binder are represented in Table 2.

Table 2: Binder properties [17].

Properties	Binder Components		
	HDPE	PW	SA
Specific heat capacity/J·K−1·kg−1	2200	2700	1700
Thermal conductivity/W·m−1·K−1	0.30	0.14	0.35
Temperature(T_{ox}) K	463	373	383
Zero-shear-rate viscosity (η_∞) Pa.s	300	0.009	0.007
Activation energy (E_x) /j.mol-1	26300	4400	0

The simulation focused to estimate the mixing index (λ) from the local shear rate $(\dot{\gamma})$ and the local intensity of the vorticity (ω') expressed as [18]:

$$\lambda = \frac{\dot{\gamma}}{\dot{\gamma} + \omega'} \tag{11}$$

3. Results and discussion

3.1. Results

The simulation was implemented to accommodate 20 steps within the duration of the each run. This allows monitoring at every 9°covered by the rotor rotation from the reference axis. Three trials were carried out and results are presented in Fig. 5 to 8.
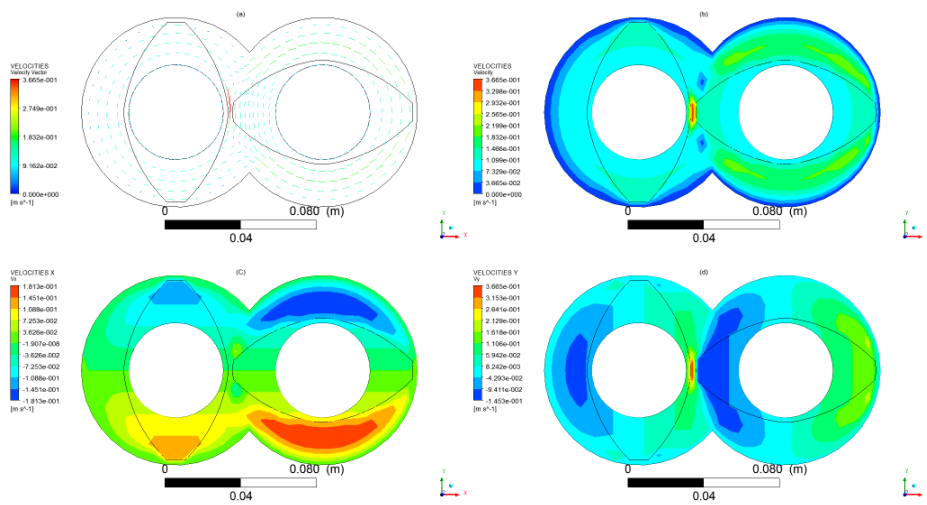
Fig. 5. (a) Velocity vector; (b) flow velocity; (c) Velocity along x- direction; (d) Velocity along y-direction at 30 rpm.
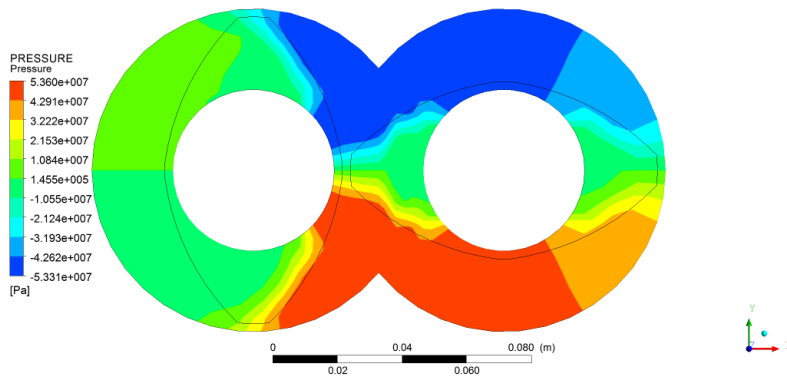
Fig. 6. Contour plot of pressure of flow domain at 30 rpm.
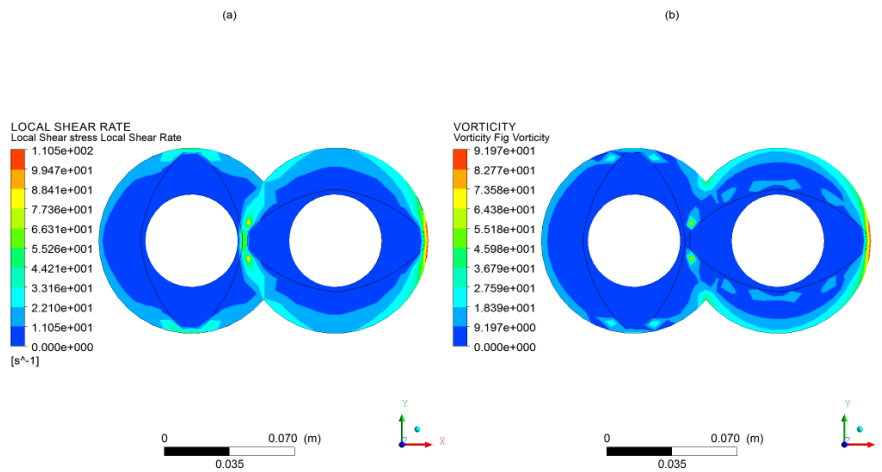
Fig. 7. (a) Local shear rate; (b) local intensity of the vorticity at 30 rpm.
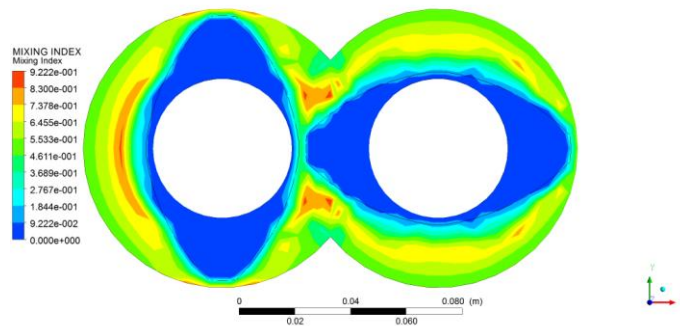
Fig. 8. Mixing index at 30 rpm.

3.2. Discussion

Fig. 5a, shows the velocity vector of the co-rotating twin-screw and fluid flow within the mixing chamber with a maximum velocity of 0.3665 ms^{-1} in a counter clockwise direction as illustrated by the vectors profile. This is a prediction of velocity distribution across the twin-screw profile within the flow domain. Fig. 5b is a colour map of the velocity showing the magnitudes according to different colours and the maximum velocity was found to be 0.35368 ms^{-1}. In addition, Fig. 5c depicts velocity along the *x*-direction (V_x) with a minimum of -0.1813 ms^{-1} and maximum of 0.1813 ms^{-1}. While, Fig. 5d depicts velocity along the *y*-direction (V_y) having a minimum value of -0.14523 ms^{-1} and maximum of 0.36647 ms^{-1}. The result of pressure prediction shown in Fig. 6 recorded high impact pressure at the lower part of the barrel towards the centre with a maximum of 53.6 MPa. Local shear rate and vorticity of the flow domain show similar trend but the local shear rate was observed to be more pronounced at the centre having a maximum value of 110. 52 s^{-1}, as shown in Fig. 7a.

The trend of the simulation results suggests the expected swapping of the screws between the two lobes in a co-rotating twin-screw mixer, which provide the required homogenous of the feedstock mix. However, the simulation trials at speed of 25 rpm and 35 rpm show an increased in velocity and pressure but less impact on the mixing index. Fig. 8 illustrates the mixing index at 30 rpm with a maximum value of 0.922. These simulation results are in good agreement with findings by other researchers [7, 11].

4. Conclusions

The physics of the flow domain were modeled using FEM based on the mixed Galerkin method and implemented with ANSYS 14.0, Fluid Flow (POLYFLOW) software. This allows a wide scope of random trial but controlled by optimisation techniques to account for efficient product design. Based on the simulation results, following conclusions can be drawn.

- The miniature mixer proposed in this paper will be a convenient bench top and suitable for micro metal injection moulding feedstock preparation. Dispersive mixing by planetary gear mixers show an efficient mixing of feedstock components.
- High mixing index value of 0.922 indicates better homogeneous mix of the feedstock which will result in quality injection molded product.
- With the increase of screw speed, the velocities along *x* and *y* direction increase which indicate better mixing feedstock materials.
- The mixer will be suitable for a wide range of materials which are hard, medium hard brittle and fibrous sample.
- Development of this mixer will enhance micro metal moulding productivity and improve production cycle time.

Acknowledgements

References

[1] A.-N. Huang, H.-P. Kuo, Developments in the tools for the investigation of mixing in particulate systems – A review, in: Advanced Powder Technology, 2014, pp. 163-173.

[2] J. Bridgwater, Mixing of powders and granular materials by mechanical means—A perspective, in: Particuology, 2012, pp. 397-427.

[3] P.M. Portillo, M.G. Ierapetritou, F.J. Muzzio, Characterization of continuous convective powder mixing processes, in: Powder Technology, 2008, pp. 368-378.

[4] B.F.C. Laurent, J. Bridgwater, Performance of single and six-bladed powder mixers, Chemical Engineering Science, 57 (2002) 1695-1709.

[5] T.A. Kingston, T.J. Heindel, Granular mixing optimization and the influence of operating conditions in a double screw mixer, in: Powder Technology, 2014, pp. 144-155.

[6] M.A. Emin, H.P. Schuchmann, Analysis of the dispersive mixing efficiency in a twin-screw extrusion processing of starch based matrix, in: J Food Eng, 2013, pp. 132-143.

[7] M.L. Rathod, J.L. Kokini, Effect of mixer geometry and operating conditions on mixing efficiency of a non-Newtonian fluid in a twin screw mixer, in: J Food Eng, 2013, pp. 256-265.

[8] K.V. Vyakaranam, J.L. Kokini, Prediction of air bubble dispersion in a viscous fluid in a twin-screw continuous mixer using FEM simulations of dispersive mixing, in: Chem Eng Sci, 2012, pp. 303-314.

[9] C. Bi, B. Jiang, Study of residence time distribution in a reciprocating single-screw pin-barrel extruder, in: Journal of Materials Processing Technology, 2009, pp. 4147-4153.

[10] F. Bertrand, F. Thibault, L. Delamare, P.A. Tanguy, Adaptive finite element simulations of fluid flow in twin-screw extruders, in: Computers & Chemical Engineering, 2003, pp. 491-500.

[11] R.K. Connelly, J.L. Kokini, Examination of the mixing ability of single and twin screw mixers using 2D finite element method simulation with particle tracking, in: J Food Eng, 2007, pp. 956-969.

[12] A. Eitzlmayr, G. Koscher, G. Reynolds, Z. Huang, J. Booth, P. Shering, J. Khinast, Mechanistic modeling of modular co-rotating twin-screw extruders, International journal of pharmaceutics, 474 (2014) 157-176.

[13] P. Müller, J. Tomas, Simulation and calibration of granules using the discrete element method, in: Particuology, 2014, pp. 40-43.

[14] M. Combarros, H.J. Feise, H. Zetzener, A. Kwade, Segregation of particulate solids: Experiments and DEM simulations, in: Particuology, 2014, pp. 25-32.

[15] J. Bridgwater, Mixing of particles and powders: Where next?, in: Particuology, 2010, pp. 563-567.

[16] K. Kohlgrüber, M. Bierdel, Co-rotating Twin-screw Extruders: Fundamentals, Technology, and Applications, Carl Hanser Publishers, 2008.

[17] W. Fang, X. He, R. Zhang, S. Yang, X. Qu, The effects of filling patterns on the powder–binder separation in powder injection molding, in: Powder Technology, 2014, pp. 367-376.

[18] A. Ficarella, M. Milanese, D. Laforgia, Numerical study of the extrusion process in cereals production: Part I. Fluid-dynamic analysis of the extrusion system, J Food Eng, 73 (2006) 103-111.

6th BSME International Conference on Thermal Engineering (ICTE 2014)

Effect of Quenching Medium on Hardness of Carburized Low Carbon Steel for Manufacturing of Spindle Used in Spinning Mill

Md. Arefin Kowser*, Md. Abdul Motalleb**

*Associate Professor, Department of Mechanical Engineering, Dhaka University of Engineering & Technology, Gazipur,
Country: Bangladesh
Email: nadimduet@yahoo.com
** Post-Graduate student, Department of Mechanical Engineering, Dhaka University of Engineering & Technology, Gazipur
Country: Bangladesh
Email: abdul.motalleb@gmail.com

Abstract

Heating or cooling of a metal can change its microstructure, which causes variations in the mechanical and physical properties and affects the behavior of the metal in processing and operation. By using the heat treatment, metal properties can be improved for the application in engineering fields. There are different spare parts used for different purposes collected from foreign countries in Spinning Mills available machine in Bangladesh. Spindle is an important part of spinning mills. The locally available raw materials are low carbon steel from which spindle can be made through property development by heat treatment. But to achieve the desire hardness and strength it is difficult to get the spindle without bending in heat treatment due to the length of spindle is too high to its diameter. Time and temperature of carburizing, quenching is the very sensitive issue to get a sound job with desire properties. In this research, quenching temperature, time and medium was considering in heat treatment process. Finally the spindle was prepared through heat treatment with desired properties comprising in a practical field of spinning mill. All the process was explained clearly for the preparation of spindle for spinning mill from locally available low carbon steel.

Keywords: Spindle, Pack Carburizing, Quenching, Tempering, Martensite, Rockwell Hardness Test, Microstructure;

---

* Corresponding author. Tel.: +8801754262832; fax: +88029204710.
E-mail address: nadimduet@yahoo.com

1. Introduction

Spindle is an important part of spinning mills. As its name is spindle, it is rotating at high speed at 3000-3500 rpm. The high hardness and high strength is required for a spindle which is achieved by heat treatment of steel. There is lot of spinning mills developed in Bangladesh in a decade and their requirement of spindle is huge in quantity. But unfortunately no supporting industry for manufacturing of spindle is developed in our country. Due to proper research and raw materials, this area is undeveloped and completely import dependent. The imported spindle is made by EN-31 metal containing some alloying elements. In Bangladesh, steel mills are produced only structural steel containing maximum 0.35% carbon which is known as low carbon steel. Locally available low carbon steel has no hardness in the sense of mechanical usages. So, the purpose of this project is to improve hardness (spindle which has been shaped using the locally available low carbon steel material) through the heat treatment process and to implement it to the machine functional area to meet the same purpose as it done earlier using the foreign spindle part. The maximum diameter of the spindle is 18.5 mm and the length is 463 mm. As the surface area is high, there is a lot of propensity to bend the job during quenching. So the selection of quenching medium is very important for quality job without bending.

Heat treatment of a metal can change its microstructure, which increases the tensile strength, hardness etc. [1]. Low carbon steel containing 0.1% to 0.18% carbon, which will not respond to direct hardening [2]. Carburizing is the addition of carbon to the surface of low-carbon steels at temperatures within the austenitic region of the steel concern, which generally is between 850°C and 950°C. Within this temperature range austenite, which has high solubility for carbon, is the stable crystal structure. Hardening is accomplished when the subsequent high-carbon surface layer is quenched to form martensite so that a high-carbon martensitic case with good wear and fatigue resistance is superimposed on a tough, low-carbon steel core [3]. Carbon diffusivity in austenite varies both with carbon concentration and carburizing temperature [4-8]. The study of process parameters in metals during heat treatment has been of considerable interest for some years [9-13].

2. Experimental Investigations

In this research work, the low carbon steel bar was collected from local market and a spindle was collected from local jute spinning mill. Then hardness measurement and microstructural observations were carried out.

Experimental procedure can be described in different works are:
2.1 Preparation of Spindle

As the length of the spindle is larger than the diameter it is better to select the original spindle for experiment. Low carbon steel solid round shaped shaft is purchased from a reliable local source and then the material is shaped and finished as per design.

The designed spindle used in jute spinning mill is shown in Figure1.
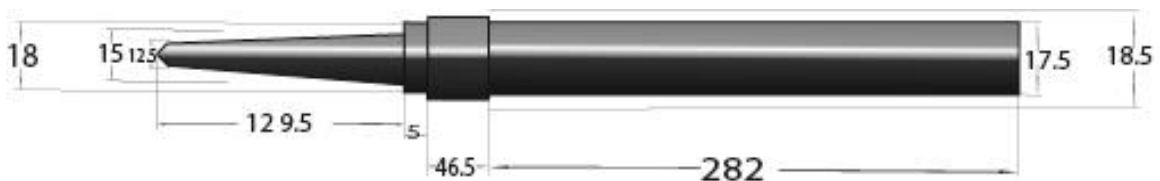
Fig.1: Design of Spindle (all dimensions are given in mm)

2.2 Heat Treatment

Before the heat treatment it is required to increase the carbon content in the low carbon steel sample. Carburizing is the addition of carbon to the surface of low-carbon steels at temperatures generally between 850 °C and 950 °C (1560 °F and 1740 °F), at which austenite, with its high solubility for carbon, is the stable crystal structure. Hardening is accomplished when the high-carbon surface layer is quenched to form martensite so that a high-carbon martensitic case with good wear and fatigue resistance is superimposed on a tough, low-carbon steel core [16]. The main objective

of this project is to carry out the heat treatment of low carbon steel material and then to compare the mechanical properties before and after heat treatment. There are various types of heat treatment processes are adopted.

2.2.1 Pack Carburizing

To increase the carbon content in the surface, pack carburizing process was used for its low cost. The spindle specimen was heated up to 900°C in a chamber furnace and the holding time was 4 hours at that temperature. Then the furnace was switched off so that the specimen temperature will decrease with the same rate. The specimen was taken out from the furnace after 48 hours when the furnace temperature had already reached at room temperature. Considering a production shift (8 hours) and required case depth, the carburizing temperature was selected from the following table 1.

Table 1: Case depth of deposition with respect to time and temperature [17]

Time (Hr) at Temp.°C	Case depth in mm				
	700°C	900°C	925°C	950°C	980°C
1	0.45	0.55	0.65	0.75	0.85
2	0.55	0.75	0.9	1.05	1.2
3	0.65	0.95	1.1	1.3	1.5
4	0.75	1.1	1.25	1.5	1.75
5	0.85	1.2	1.4	1.7	1.95
6	1.1	1.3	1.55	1.85	2.15
8	1.25	1.5	1.8	2.1	2.45
10	1.4	1.7	2.0	2.35	2.75

Sample was taken out from furnace. Time-Temperature curve during carburizing is shown in figure 2.
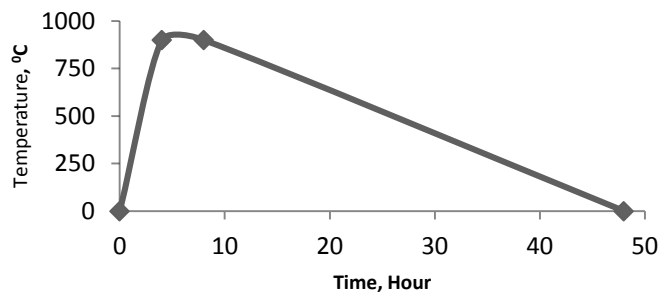
Fig. 2: Time-Temperature curve of carburizing

2.2.2 Quenching

Two types of quenching medium (oil and water) were used to quench the sample. The specimen was heated to the temperature of 850°C and was allowed to homogenize at that temperature for 10 minutes. After 10 minutes, the specimen was taken out from the furnace and directly quenched in oil and water for rapid cooling.

2.2.3 Tempering

Tempering is used to reduce the internal stress developed in quenching. For this, the specimen was heated to 150°C and hold for 1 hour to reduce internal stress. After the heat treatment specimens were cooled in tempering furnace. Time-Temperature curve of tempering is shown in Figure 3.
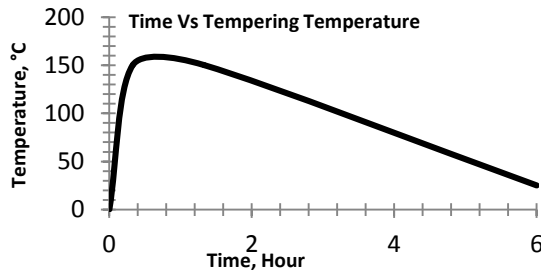
Fig. 3: Time-Temperature curve during Tempering

2.3.1 Hardness Test

Before heat treatment the specimen hardness was measured by means of Rockwell hardness tester in C scale which was zero in actual. Imported spindle hardness was also measured. The hardness testing was conducted at room temperature.

Water quenched spindle shows high hardness and oil quenched spindle shows lower but at working level. Hardness comparison among the oil quenched, water quenched and imported spindle samples are shown in figure 4.
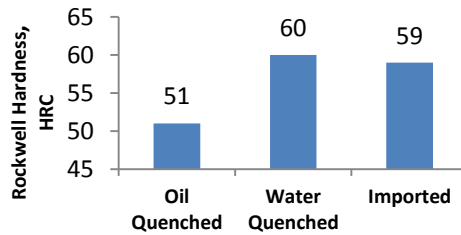
Fig. 4: Hardness comparison among oil, water quenched and imported spindle sample

2.3.2 Compressive Strength Measurement

The compressive strength is measured by compressive test which is carried out by a universal testing machine (UTM). In present experiment the compressive test was carried out on before heat treated and after heat treated sample. Parameter were settled during compression test is shown as following table 2.

Table 2: Experimental condition during compression test by Universal Testing Machine (UTM).

Parameter	Experimental condition
Cross head Speed (mm/min)	0.05
Loading Range (KN)	0-50
Humidity (%)	70
Temperature (°C)	24

The Engineering and True Stress Vs Strain curve of compression test for before and after heat treatment (oil quenched) curve is shown in Figures 5 (a), (b) and combined curve is shown in Figure 5(c) which shows the true stress is larger than the engineering stress for the same strain. The engineering stress was converted to true stress by using the equation 1 and engineering strain was converted to true strain by using the equation 2.

$$\sigma_T = \sigma_E (1 + \varepsilon_E) \tag{1}$$

Where, σ_T = True Stress, σ_E = Engineering Stress and ε_E = Enginering Strain.

$$\varepsilon_T = \ln (1 + \varepsilon_E) \tag{2}$$

Where, ε_T = True Strain and ε_E = Enginering Strain.
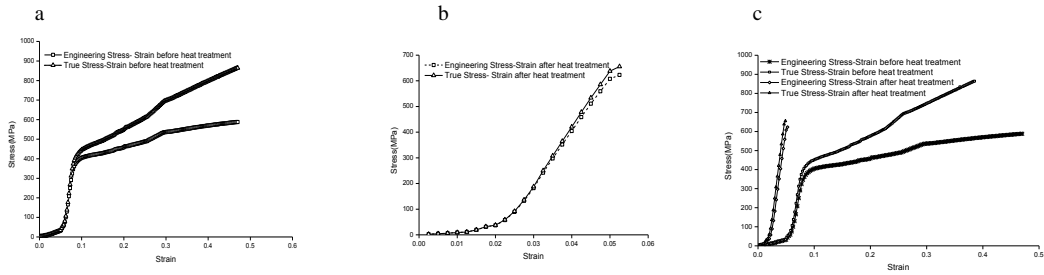
Fig. 5: Engineering and True stress Strain diagram of compression test a) before heat treatment; (b) after heat treatment (c) Combined

Engineering and True Stress-Strain diagram of compression test before and after heat treatment

2.4 Materials Composition Study

As per AISI standard, chemical composition of EN31 metal is given in table 2 [18]. Chemical composition of the locally purchased low carbon steel material and imported spindles are shown as follows in Table 3. Carbon percentage is increased almost 2.5 times after heat treatment.

Table 3: Composition of locally available low carbon steel before and after heat treatment and imported spindle material.

Sl. No.	Name of the Elements	Weight % in Low Carbon Steel before Heat Treatment	Weight % in Low Carbon Steel after Heat Treatment	Weight % in Imported Spindle
1	Carbon (C)	0.2930	0.6842	1.30
2	Silicon (Si)	0.2329	0.1918	0.30
3	Manganese (Mn)	1.2607	1.0231	0.50
4	Sulphur (S)	0.0329	0.0296	0.025
5	Phosphorous (P)	0.0485	0.0407	0.024
6	Chromium (Cr)	0.0716	0.0556	1.40
7	Nickel (Ni)	0.0742	0.0530	-
8	Copper (Cu)	0.2315	0.1965	-

2.5 Microstructural Study

Microstructural study was carried out of the locally purchased low carbon steel material before and after heat treatment and imported spindles. Polishing work was carried out by various grades of emery paper and finally polished by alumina powder in grinding wheel. The polished samples were etching with 2% nital. Then the microstructure was observed by metallurgical microscope. Figure 6 shows the microstructure of low carbon steel before and after heat treatment which contains (a) low pearlite and high ferrite structure.

Fig. 6: Microstructure of low carbon steel (a) before heat treatment (b) after heat treatment (oil quenched) (c) after heat treatment (water quenched). Ethced with 2% Nital (Magnification 400x)

3. Discussion

The hardness of spindle was increased by heat treatment process. The cooling rate during quenching as shown in figure 7(a) and the alloying elements as shown in figure 7(b) are one of the main factor to increase the hardness. The carburizing temperature and time is also influence the hardness of spindle. If the carburizing temperature increases then the solubility of carbon in iron is also increases but at the same time austenite grain size increases. As the spindle length is high there is a probability of bending during carburizing at high temperature. The selection of carburizing temperature at 900^0C and time 4 hours also cover a shift production (8 hours) of the factory. To protect the distortion and bending defect the quenching temperature was selected at 850^0C. The holding time of quenching was selected on basis of the diameter of the spindle as per minute per inch diameter.

The cooling rate of water is higher than the oil. From the figure 7(a) it seems that the formation of martensite is depend on the cooling rate. Martensite is a supersaturated solid solution of carbon trapped in a body-centered tetragonal structure. This highly distorted lattice structure is the prime reason for the high hardness of martensite. The water quenched spindle was harder than the oil quenched as cooling rate is higher which also persist to trend it to distort and bend. In visual inspection the water quenched spindle was bended and the oil quenched spindle was straight. As the oil quenched spindle was found straight, the compressive strength was measured only oil quenched spindle. The compressive strength was increased after heat treatment.
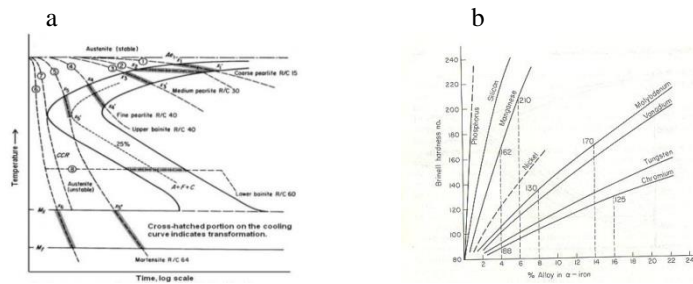
Fig. 7: (a) Cooling curves superimposed a hypothetical I-T diagram; (b) Effect of alloying elements on hardness of steel.

The imported spindle was made by EN31 metal which contains high carbon and nickel. These two elements increase the hardness and wear resistance. That is why the imported spindle has high hardness. In Bangladesh there is no manufacturing company to produce the low alloy steel or high carbon steel. But the available structural steel is low carbon steel from which the spindle will be manufactured by following the heat treatment process. The properties of spindle manufactured from locally available low carbon steel and imported spindle is compared in table 4.

Table 4: Comparison of improved local material with foreign material

Ser No	Key Elements	Locally Developed Spindle	Imported Spindle	Remarks
1	Durability	Durable	Durable	Using in Anwar Jute Spinning Mill Ltd.
2	Quality	Meets requirement.	Meets requirement.	Do
3	Availability	Available whenever require as it is possible to make locally.	Not possible to provide any time as it came from foreign countries.	Any time available
4	Stock Maintenance	Stock maintenance does not require as it is easily available.	Requires always keeping a lot amount in stock as it came from foreign countries.	No investment in stocking the spindle as it is locally available
5	Price	Comparatively very low price than imported	Price is comparative higher than the locally made.	About 3 times lower than imported

After heat treatment, the grinding operation was carried out for the smooth finishing of spindle. A finished spindle improved from low carbon steel is shown in figure 8.

Fig. 8: Improved finished spindle

4. Conclusion

It is recommended to oil quenched for this type of spindle. Heat treatment of low carbon steel was carried out in this research. The spindle was prepared and then heat treatment process of pack carburizing, quenching and tempering has been conducted and a mechanical property has been studied and microstructure was observed before heat treatment and after the heat treatment of the spindle. There were three spindles for water quenching and three spindles for oil quenching were chosen and the quenching operation was carried out. As the cooling rate of water is higher than the oil, the hardness of water quenched spindle was higher than the oil quenched. On the other hand, the water quenched spindle was bended and the oil quenched spindle was found straight. The development of a spindle with a suitable hardness without any bending is the main aim of this project. So the oil quenched spindle used to the machine functional area to check the performance of the spindle and after the consecutive operation of the machine it was found that the improved hardness and strength meets the user requirement with compliance to the smooth rotating quality. It can be concluded that locally available low carbon steel can be used for the preparation of spindle for spinning mill using the proper heat treatment process.

References

[1] Murugan V.K., Mathews P. K., "Effect of Tempering Behavior on Heat Treated Medium Carbon (C35 Mn75) Steel", International Journal of Innovative Research in Science, Engineering and Technology, Vol. 2, Issue 4, April 2013.
[2] Jain R.K, Gupta S.C, "Production Technology", 12th Edition, Khanna Publishers.
[3] Krauss G. Principles of Heat Treatment of Steel, American Society for Metals, Ohio, 1980, pp. 209 219.
[4] Goldstein J.I., Moren A.E. Diffusion Modeling of the Carburization Process, Metallurgical and Materials Transactions A, 1978, 9 (11), pp. 1515-1525. Parrish G 1999.
[5] Totten G.E., Howes M.A.H., Steel Heat Treatment Handbook, 2nd Edition, Marcell Dekker, Inc., New York, Chapter 7, 1997.
[6] Agren J., Revised Expression for the Diffusivity of Carbon in Binary Fe-C Austenite, Scripta Metallurgica, 1986, 20(11), pp. 1507-1510.
[7] Asimow R.M. Analysis of the Variation of the Diffusion Constant of Carbon in Austenite with Concentration, Transactions of AIME, 1964, 230(3), pp. 611-613.
[8] Denis S., Coupled temperature stress, phase transformation calculation model numerical illustration of the internal stresses evolution during cooling of a eutectoid carbon steel cylinder, Metallurgical Transaction A, 1987, 18A, pp. 1203-1287.
[9] Leblond J.B., Mathematical modeling of transformation plasticity in steels I: Case of ideal plastic phases II: Coupling with strain hardening phenomena, International Journal of Plasticity, 1989, 5, pp. 551-591.
[10] Wang K.F., Chandrasekar S., Yang H.T.Y., Experimental and computational study of the quenching of carbon steel, International Journal of Manufacturing Science and Engineering, 1997, 119, pp. 257-265.
[11] Liu C.C., Xu X.J., Liu Z., A FEM modeling of quenching and tempering and its application in industrial engineering, International Journal of Finite Elements in Analysis and Design, 2003, 39, pp. 1053-1070.
[12] Xu D.-H., Kuang Z-B., A study on the distribution of residual stress due to surface induction hardening, International Journal of Engineering Materials and Technology, 1996, 118, pp. 571-575.
[13] Shewmon G.P., Diffusion in solids, series in material science and Engineering, Mc Graw Hill, Tokyo, 1963.

6th BSME International Conference on Thermal Engineering (ICTE 2014)

Thermal Investigation of Vortex Generated Green Coolant on Surface Texture for Drilling Process

Anayet U. Patwari[a,]*, M. A. Habib[a], Md. S.I. Chowdhury [a], Rana Md. Hassnain Akram [a]

[a]Dept. Mechanical and Chemical Engineering, Islamic University of Technology (IUT), Bangladesh

Abstract

High material removal rate, better surface finish and low tool wear are the major needs in different machining processes. Moreover, in order to fulfill those requirements researchers need to focus not only on the quality but also on the ecofriendly nature of machining. Now-a-days, environmental safety takes the foremost priority to industries and people in general. For this reason, this paper attempts in effectively applying vortex generated green coolant for CNC drilling process utilizing an eco-friendly system. In this study, vortex generated cold air were used as green coolant for CNC drilling process and compared with standard liquid coolant and dry condition. In order to investigate the effectiveness of the green coolant different machining conditions were used to get a better surface finish. It has been observed that the vortex generate green coolant shows better surface finish for different range of cutting conditions with respect to both standard liquid coolant and dry condition. At the same time, this process is environment friendly and economic as well.

© 2015 The Authors. Published by Elsevier Ltd.
Peer-review under responsibility of organizing committee of the 6th BSME International Conference on Thermal Engineering (ICTE 2014).

Keywords: CNC Drilling; Vortex tube; Coolant; Surface roughness

1. Introduction

High speed machining of steel inevitably produces high cutting temperature at the work piece-cutting tool contact point. Such high temperature adversely affects the tool life and product quality. Different types of cutting fluids are used to address this temperature increase. However, there has been increasing concerns regarding the use of cutting

fluids in the production, due to the costs related to the fluids, ecological issues, human health and so on. Two techniques that have been intensively experimented on are: dry cutting (cutting without any fluid, also known as ecological machining) and minimum quality lubrication, MQL, (cutting with a minimum quantity of fluid).

Sreejith et al. [1] studied and discussed the recent advancements in dry machining. They compiled the different parameters required for dry machining and also discussed about the use of this technique for machining different materials. Dudzinski et al. [2] reviewed the details of development of dry machining and high speed cutting of Inconel 718 alloy. They focused on the recent work and advances concerning machining of this material. They also explored some solutions to reduce the use of coolants and different coating techniques to enable a move towards dry machining. Dhar et al. [3] compared the mechanical performance of MQL to completely dry lubrication for the turning of AISI-1040 steel. The comparison was based on experimental measurement of cutting temperature, chip reduction coefficient, cutting forces, tool wears, surface finish, and dimensional deviation. Results indicated that the use of near dry lubrication leads to lower cutting temperature and cutting force, favourable chip–tool interaction, and dimensional deviation. Change in the chip–tool and work–tool interactions helped in reducing friction, built-up edge formation, thermal distortion of the work and wear of the cutting tool. Kelly et al. [4] studied the effect of minimal lubrication machining of aluminium alloys. They investigated into various methods of cutting fluid application with the objective of deriving the optimum cutting condition for the drilling of cast aluminium alloys. Results showed that it is nearly impossible to drill aluminium without a cutting fluid, because of its unfavourable dry cutting properties. It was also found that flood lubrication is superior for lower cutting speeds and feed rates, whilst mist application is superior for higher cutting speeds and feed rates. Braga et al. [5] used minimum quantity of lubricant (MQL) and a diamond coated tool in the drilling of aluminum–silicon alloys. They compared the performance of the uncoated and diamond coated carbide drills, using minimal lubrication and abundant soluble oil as a lubricant in the drilling of aluminum–silicon alloys (A356). The results showed an irregular wear in the surface of the diamond coated drill and a decrease in the quality of the hole made by it, compared to the uncoated drill. Results showed that MQL system presented either similar or better quality than those obtained with flood of abundant soluble oil. Dhar et al. [6] studied the influence of minimum quantity of lubrication (MQL) on cutting temperature, chip and dimensional accuracy in turning AISI-1040 steel. The results have been compared with dry machining and machining with soluble oil as coolant. The experimental results indicate that such MQL enables substantial reduction in the cutting temperature, dimensional inaccuracy depending upon the levels of the cutting velocity and feed rate. It was also noted that the chip formation and chip–tool interaction become more favorable under MQL condition. Zeilmann et al. [7] studied the effect of temperature during drilling of Ti6Al4V with minimal quantity of lubricant. The lubricant was applied either with an external nozzle or internally through the drill. The results showed significant benefits with MQL applied internally through the tool. For drilling with MQL applied with an external nozzle, the process was constrained to small depths and limited with reference to the requirements of the surface quality of the hole. Davim et al. [8] made experimental investigations on drilling of aluminium under dry, minimum quantity of lubricant and flood-lubricated conditions. The experiments were planned based on orthogonal arrays. An analysis of variance (ANOVA) was carried out to check the validity of the proposed parameters and also their percentage contributions. Results showed that cutting power and specific cutting force were higher for dry drilling compared to other two. Results also showed that with a proper selection of the range of cutting parameters, it is possible to obtain performances similar to flood lubricated conditions by using MQL.

This paper investigates a novel technique of using vortex generated cold air as coolant in drilling process instead of liquid coolant and dry condition. A unique portable vortex tube was developed for this purpose. This vortex generated green coolant shows great promise in reducing surface finish for different range of cutting conditions. The process is environment friendly and economic as well.

2. History and working principle of vortex tube

The vortex tube was invented quite by accident in 1928. George Ranque, a French physics student, was experimenting with a vortex-type pump he had developed when he noticed warm air exhausting from one end, and cold air from the other. A vortex tube uses compressed air as a power source, has no moving parts, and produces hot air from one end and cold air from the other (Fig. 1.). The volume and temperature of these two airstreams are adjustable with a valve built into the hot air exhaust. Temperatures as low as -50°F (-46°C) and as high as +260°F

(127°C) are possible. Compressed air is supplied to the vortex tube and passes through nozzles that are tangent to an internal counter bore. These nozzles set the air in a vortex motion. This spinning stream of air turns 90° and passes down the hot tube in the form of a spinning shell, similar to a tornado. A valve at one end of the tube allows some of the warmed air to escape. What does not escape, heads back down the tube as a second vortex inside the low-pressure area of the larger vortex. This inner vortex loses heat and exhausts through the other end as cold air.

While one airstream moves up the tube and the other downs it, both rotate in the same direction at the same angular velocity. That is, a particle in the inner stream completes one rotation in the same amount of time as a particle in the outer stream. However, because of the principle of conservation of angular momentum, the rotational speed of the smaller vortex might be expected to increase. But in the vortex tube, the speed of the inner vortex remains the same. Angular momentum has been lost from the inner vortex. The energy that is lost shows up as heat in the outer vortex. Thus the outer vortex becomes warm, and the inner vortex is cooled [9].

(a)   (b)
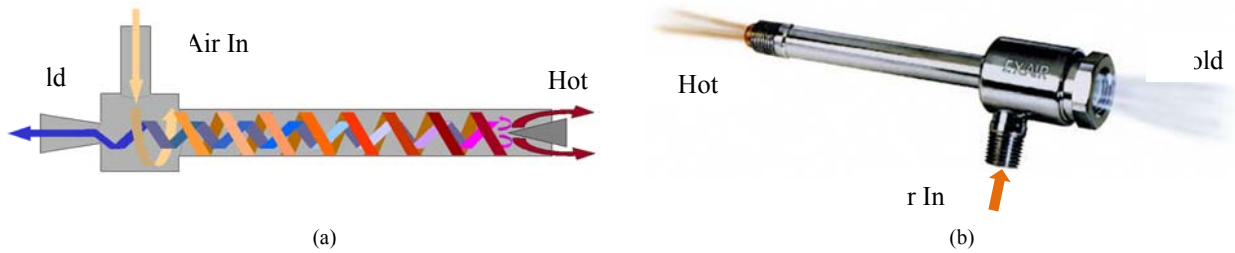
Fig. 1. Separation of a compressed gas into a hot stream and a cold stream

3. Experimental Setup and Methodology

3.1. Experimental Setup

For the drilling process, Z K 2512-3 CNC drilling machine (Fig. 2.) was utilized. Its maximum drilling capacity was 25mm and X, Y and Z axis travel length were 250mm, 180mm and 150mm respectively. The advantage of this machine is that it has a built in computer terminal and software. Thus, the outputs of the model can be programmed using this software and input into the machine.

To apply the cold air into the drilling process a novel portable vortex tube (Fig. 3.) was developed. The vortex tube pipe was made up of PVC. The compressed air inlet lets in the compressed air into the swivel chamber which sets the air into vortex motion. Hot and cold air was then obtained at the hot and cold air end respectively. The temperature of the cold air was able to reach as low as 10ºC. The pressure of the compressor was 6 bars. Fig. 4. shows the experimental setup for the drilling process.

Fig. 2. Photograph of the CNC drilling machine

Fig. 3. Photograph of the developed Vortex tube
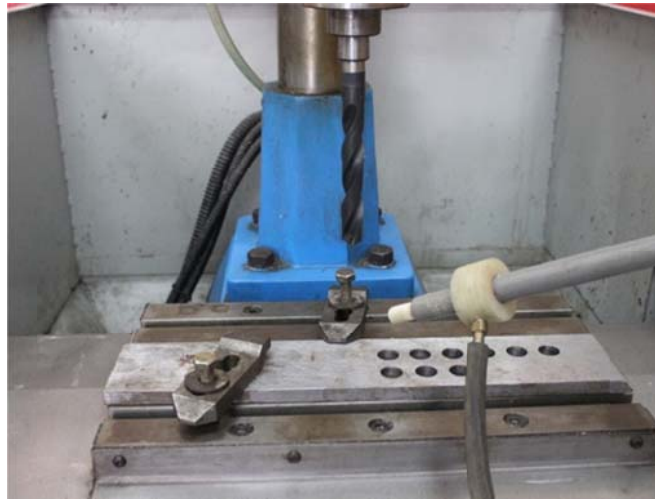
Fig. 4. Photograph of the Experimental Setup

3.2. Methodology

   In this study, different combinations of cutting conditions were considered for carrying out the experiments under three coolant conditions: Dry, Liquid and vortex generated cold air. Table 1 shows the experimental process variables for the study. Experiments were carried out by through drilling mild steel bars of thickness 20mm. For each coolant condition, 9 experiments were conducted with different combinations of cutting parameters. Temperatures were measured for all the experiments and were averaged to obtain the coolant temperature. Surface roughness of the machined surface (Fig.5) was then measured. To minimize errors, 5 surface roughness values were taken for each machined surface at different points and were then averaged to obtain the surface roughness values. Surface roughness values were measured with Mitutoyo Surftest SJ-210 contact profilometer (Fig.6). Its measuring range in x axis is 17.5 mm and measuring range/resolution in z axis (detector) is 360μm / 0.02μm.

Fig. 5. Photograph of the through drilled hole

Fig. 6. Mitutoyo Surftest SJ-210 contact profilometer

Table 1. Experimental process variables

Process Variables		
Coolant	Feed Rate (mm/min)	Speed (RPM)
Dry Condition		
Liquid coolant	5, 10, 15	500, 1000, 1500
Cold air from vortex tube		

Table 2.Experimental results for surface roughness for different coolant.

S. No.	Coolant	Speed (rpm)	Feed Rate (mm/min)	Average Coolant Temp (°C)	Average Surface Roughness (µm)
1	Dry	500	5	35	3.31
2			10		3.45
3			15		3.74
4		1000	5		3.23
5			10		3.97
6			15		3.80
7		1500	5		1.92
8			10		1.88
9			15		2.61
`10	Liquid Coolant	500	5	30	2.88
11			10		3.20
12			15		3.50
13		1000	5		2.90
14			10		3.16
15			15		3.41
16		1500	5		1.79
17			10		1.79
18			15		2.30
19	Cold Air from Vortex tube	500	5	10	2.35
20			10		2.83
21			15		3.16
22		1000	5		2.70
23			10		2.60
24			15		2.91
25		1500	5		1.54
26			10		1.66
27			15		2.04

4. Results and Discussion

Table 2 shows the experimental results of average surface roughness and coolant temperature. Fig. 5. shows the photograph of a through drilled hole using vortex tube generated cold air. The effect of rotational speed and feed rate on surface roughness for different coolant is discussed below:

4.1. Effect of rotational speed on surface roughness

Fig. 7. (a), (b) and (c) shows the effect of rotational speed on surface roughness for the feed rate of 5 mm/min, 10 mm/min and 15 mm/min. Figures show that the roughness values for a constant rotational speed increases with the increase of feed rate. Moreover, the roughness values for low rotational speed are comparatively higher than higher rotational speed. If we compare surface roughness for the three types of coolant, then it is clear that the machined surface roughness by using the vortex generated coolant is less than the other two coolants. This proves that the high pressure vortex generated cold air is more capable of removing heat from the cutting zone than the other two's. The surface roughness improvement by vortex cold air for fig. 7 (a) and 7 (b) is better than fig. 7 (c). This is because; in fig. 7 (c) the rotational speed is 1000 rpm, which is relatively higher, because the machining time is lower. The effect of vortex cold air in comparison to other coolant conditions is less due to lower machining time.
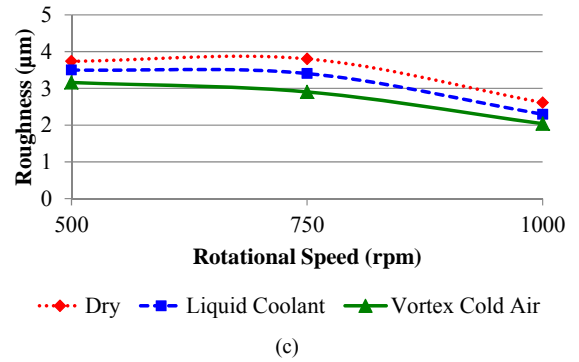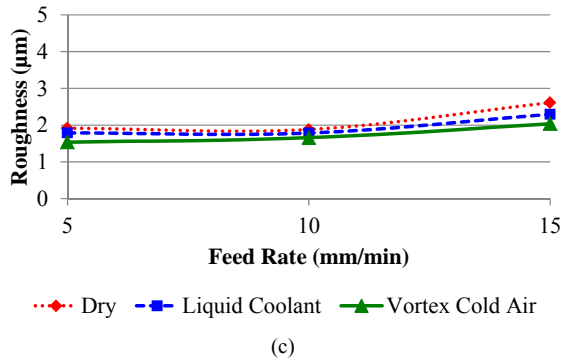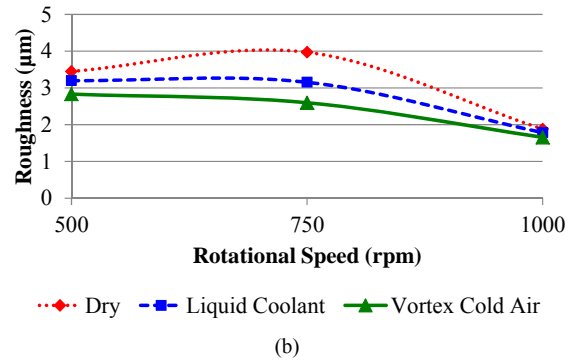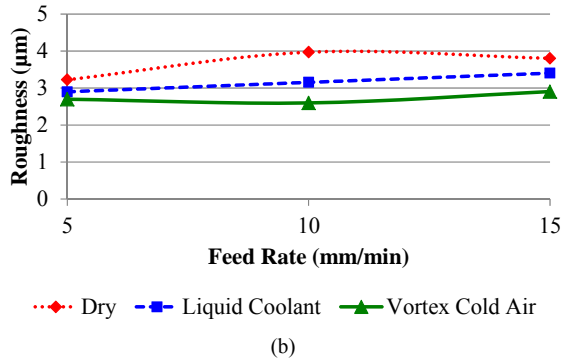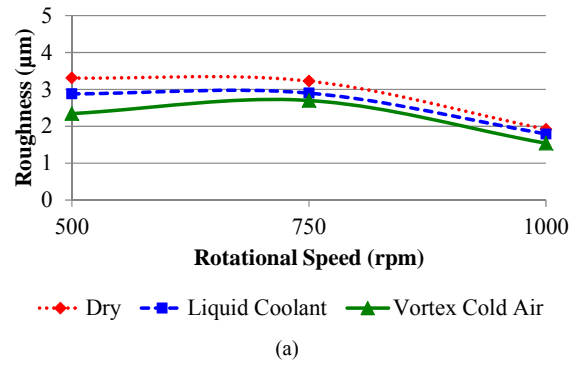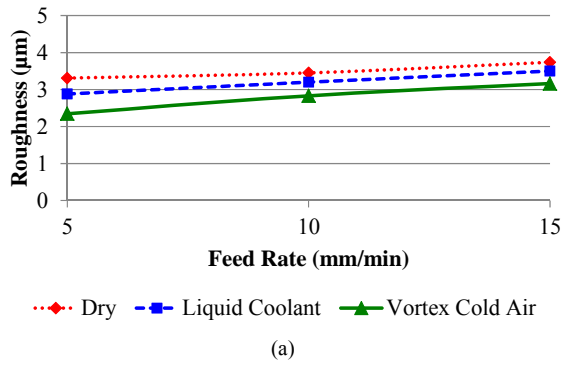
Fig. 7. Effect of feed rate on surface roughness for different rotational speeds (a) 500 rpm; (b) 750 rpm; (c) 1000 rpm

Fig. 8. Effect of rotational speed on surface roughness for different feed rates (a) 5 mm/min; (b) 10 mm/min; (c) 15 mm/min

4.2. Effect of feed rate on surface roughness

Fig. 8. (a), (b) and (c) shows the effect of feed rate on surface roughness for the rotational speed of 500 rpm, 750 rpm and 1000 rpm. Figures show that with a constant feed rate the roughness value decreases with the increase of rotational speed. At the same time, it can be observed from the figures that the roughness values increase with the increase of feed rate. The most observable phenomenon in these figures is that the surface roughness by using vortex generated cold air is lesser that the other two coolants used in the experiments. This is because, the average temperature of the vortex generated cold air is less than other coolants. For this reason, the thermal gradient for vortex generated cold air is higher. This causes the effective cooling for the machining zone. Finally, it gives better surface roughness for this current experimental setup.

5. Conclusions

Vortex tube is a simple and attractive method for producing eco-friendly coolant. In this study, a vortex tube is first fabricated in a simple way and then a set of experiments are conducted in order to examine the performance of vortex generated cold air as a coolant. The machined surface roughness by the vortex generated cold air is then compared with machining using the dry and liquid coolant. In addition to the improvement of surface roughness, vortex generated cold air is green, environment friendly and easy to handle. The fabrication of the vortex tube used in this experiment is easy and economical. If the input air pressure and the structure of the vortex tube can be improved, then the surface roughness will be better than the achieved ones. However, these can lead to increase in production cost.

References

[1] P.S. Sreejith, B.K.A. Ngoi, Dry machining: Machining of the future, Journal of Materials Processing Technology 101 (2000) 287-291.
[2] D. Dudzinski , A. Devillez , A. Moufki, D. Larrouquere, V. Zerrouki , J. Vigneau, A review of developments towards dry and high speed machining of Inconel 718 alloy, International Journal of Machine Tools & Manufacture 44 (2004) 439–456.
[3] N.R. Dhar, M.T. Ahmed, S. Islam, An experimental investigation on effect of minimum quantity lubrication in machining AISI 1040 steel, International Journal of Machine Tools & Manufacture 47 (2007) 748–753.
[4] J.F. Kellya, M.G. Cotterell, Minimal lubrication machining of aluminium alloys, Journal of Materials Processing Technology 120 (2002) 327–334.
[5] D.U. Bragaa, A.E. Dinizc, G.W.A. Mirandab, N.L. Coppinic, Using a minimum quantity of lubricant (MQL) and a diamond coated tool in the drilling of aluminum–silicon alloys, Journal of Materials Processing Technology 122 (2002) 127–138.
[6] N.R. Dhar a, M.W. Islam, S. Islam, M.A.H. Mithu, The influence of minimum quantity of lubrication (MQL) on cutting temperature, chip and dimensional accuracy in turning AISI-1040 steel, Journal of Materials Processing Technology 171 (2006) 93–99.
[7] R.P. Zeilmann, W.L. Weingaertner, Analysis of temperature during drilling of Ti6Al4V with minimal quantity of lubricant, Journal of Materials Processing Technology 179 (2006) 124–127.
[8] J.P. Davim, P.S. Sreejith, R.Gomes, C. Peixoto, Experimental studies on drilling of aluminium (AA1050) under dry, minimum quantity of lubricant, and flood-lubricated conditions, Journal of Engineering Manufacture 220 (2006) 1605-1611.
[9] Vortex Tube and Spot Cooling Products, Exair, http://www.exair.com/

6th BSME International Conference on Thermal Engineering (ICTE 2014)

Application of the spray quenching to T6 heat treatment of thick A6061 hollow cylinders

Hisayoshi Soejima[a], Yuichi Mitsutake[b]*, Suhaimi Illias[a], Koutarou Tsubaki[a] and Masanori Monde[c]

[a]Department of Mechanical Engineering, Saga University, 1 Hojo-machi, Saga-shi, Saga, 840-8502, Japan
[b]Institute of Ocean Engergy, Saga University, 1 Hojo-machi, Saga-shi, Saga, 840-8502, Japan
[c]International Research Center for Hydrogen Energy, Kyushu University, 744 Motooka, Nishi-ku, Fukuoka-shi, Fukuoka, 819-0935, Japan

Abstract

Aluminum allay A6061 is commonly applied T6 heat treatment and ultimate tensile strength above 300 MPa is obtained by solid solution strengthening. The T6 treatment consists of solution treatment, water quenching and artificial aging. Lower cooling rate during quenching is very important because impurity phase deposition in solution phase due to longer quenching delay results in growth of grains in the aging process and less strengthening. The quenching delay time strongly depends on boiling transition from film boiling to nucleate boiling as well as heat capacity of the solid. Stable wetted situation hardly occurs in the film boiling region and film boiling heat transfer coefficient is one or two digit lower than that of the nucleate boiling heat transfer. In this research, dip (bath) and spray quenches were applied to thick A6061 hollow cylinders to get comparable spray cooling rate with the conventional dip quenching. Temperature histories in the cylinder were measured during quenching and inside temperature distribution was estimated with inverse heat conduction analysis. After the T6 treatment, tensile test pieces were cut away from the cylinder and effectiveness of the spray quench was accessed. The spray quenching tests were done for water temperature of 10-22 ºC and the maximum total spray flow rate of 20 L/min with four or eight spray nozzles around the cylinder. For the dip quenching, test piece was soaked into well stirred water pool at a fixed temperature of 18 ºC. From the spray quench tests, the quenching delay time was difficult to keep within the allowable maximum delay time requested from existing metallurgical studies. It was found that higher water flow rate or larger number of nozzle arrangement will be required to obtain comparable cooling rate with the dip quenching result. However, each tensile test showed that the strength of spray quenched materials is almost equivalent to that of dip quenching and satisfied the minimum tensile strength of A6061-T6 regulated by JIS (Japanese Industrial Standards) B 8270.

* Corresponding author. Tel.: +81-952-28-8616; fax: +81-952-28-8587.
 E-mail address: mitutake@me.saga-u.ac.jp

1. Introduction

High strength aluminum alloys are widely used as structural materials for aircraft frames, automotive bodies, bicycle frames, high pressure vessel liners and so on. The 2000, 6000 and 7000 series aluminum alloys are hardened by temper heat treatment denoted as "T6" after hot or cold plastic machining process. The T6 heat treatment process consists of solution heat treatment, quenching and artificial aging. To ensure mechanical strength of materials, the heat treatment condition at each process is prescribed by the ASTM standards or the other national standards. It is well known that the strength of T6 heat treated material has a sensitivity of quenching delay time. When cooling rate during quenching becomes lower, impurity metal phases such as Zn, Mg, Si and Cu are deposited during quenching. Then grain size of deposited phase will grow up too much during the artificial aging process and result in less solution strengthening. Nucleation rate of the impurity phases strongly depends on temperature history in quenching.

In a workshop, solution treated A6061 materials at 535 °C are commonly quenched in a water bath (dip quenched). Transient boiling heat transfer starts from film boiling on the surface and then transits to nucleate boiling via transition boiling. The film boiling is characterized with hardly occurred liquid-solid contacts and very low cooling rate. Partial and intermittent liquid-solid contacts are allowed in the transition boiling heat transfer and the cooling rate increases as the recovery of steady wetting situation on the hot surface. And then the hot surface becomes fully wet, namely nucleate boiling situation takes place. The maximum cooling rate of quenching process is indicated just after the maximum surface heat flux point which occurs at wetted nucleate boiling situation. Therefore, the quenching delay time is strongly affected by rewetting of the surface due to boiling transition and the heat capacity of material depending on its dimension and thermal properties. The cooling rate of the quenched material is governed with the boiling heat transfer on its surface and the transient heat conduction in it.

Bergsma, et al.[1] provided the relationship between quenching delay time and mechanical properties at extensive temperature range from 200 °C to 500 °C for aluminum A6061-T6 and A6069-T6 alloys. They also reported the allowable maximum quenching delay time for each temperature at which ultimate tensile stress (UTS) and yield stress decreased 5 %. In case of A6061-T6, the allowable quenching delay time at 360 °C indicated the minimum delay time of about 10 s. That means the material temperature has to go down at 360 °C within 10 s.

Hall and Mudawar [2], Mascarenhas and Mudawar [3, 4] provided methodology estimating transient temperature change in L-shaped aluminum alloys and thick cylindrical tube during multiple spray jets quenching. They proposed 3D transient heat conduction analysis models with consideration of spray jet patterns on the complicate shape of the solid surface and empirical correlations expressing entire of spray boiling curve. They showed spatial optimization of the cooling rate by adjusting spray nozzle arrangements and volumetric flow rate.

In this study quenching of thick A6061 hollow cylinder was conducted to decide appropriate spray quenching conditions such as spray nozzles arrangement and spray flow rate. The cylinder specimen was an extended neck part cut from both ends of a Type-III hydrogen high pressure vessel which is made of a carbon fiber composite full wrap metallic liner. The liner was seamlessly made from an A6061 aluminum pipe by hot spinning machining. The liner had an axisymmetric body shape but thickness considerably changed from the thin body part to the thick neck part. The neck part has a SUS316 hollow cylinder inside which acts as an additional heat capacity to decrease in cooling rate of the A6061 cylinder during quenching. Since the conventional dip (bath) quenching technique has less controllability of cooling rate and uniform cooling temperature of materials with complicated shape, applicability of spray cooling has been considered to adopt quenching neck part of the liner by adjusting spray nozzles arrangement, spray flow rate and spray water temperature and optimize spray condition was decided for the thick A6061 cylinder. We assessed effectiveness of spray quenching with two spray nozzle arrangements by material strength test results and proposed appropriate spray nozzle arrangement.

Nomenclature

t	Time (s)
t_{d360}	Quenching delay time when local specimen temperature reached at 360 °C (s)
r	Radial position (mm)
z	Vertical position (mm)
N	Number of spray nozzles
q'	radial heat transfer rate per unit axial length (W/m)
Q_{spray}	Volumetric total spray flow rate (L/min)
R_i	Inner radius of a hollow aluminium cylinder
R_o	Outer radius of a hollow aluminium cylinder
T	Temperature (°C)

Subscripts
b	Specimen
l	Liquid water
w	Wall surface

Greek letters
θ	Angular position from the nozzle orientation (deg)
σ_B	Ultimate tensile stress (UTS) (MPa)

2. Experimental apparatus and procedure

2.1. Experimental setup

Figure 1 shows layout of the experimental apparatus which consists of three main parts, such as; data acquisition system, crucible furnace and water quenching bath. Temperature changes in a test specimen were recorded with the data logger at sampling rate of 10 Hz. The crucible furnace was used to heat the test specimen. The water quenching bath stored 200 L water which was large enough to keep raise in water temperature within 1 K during quenching. A water jet pump and a spray header were equipped in the bath. A feed water pump sucked water from the bath and supplied water to the spray header and the jet pump. The jet pump ejected strong water jet flow to stir storage water well. In case of spray quenching tests, the spray flow rate was adjusted with the flow control valve and measured with the turbine flow meter.

Figures 2(a) and (b) show layouts of the spray nozzles and the cylindrical test specimen for the spray nozzle number $N = 4$ and 8. The spray nozzles were equiangularly installed on the ring spray header. A cylindrical test specimen was
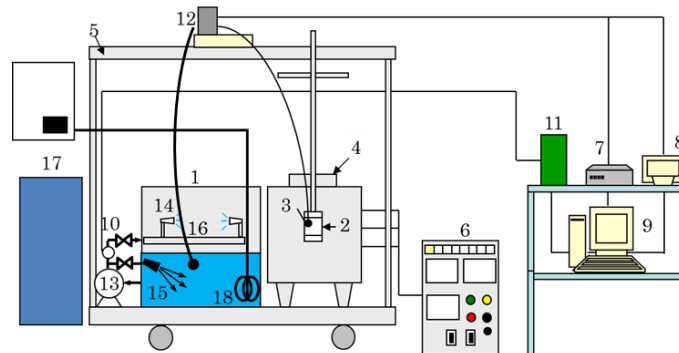
1:Water bath, 2:Test piece, 3:Thermocouple, 4:Electric furnace, 5:Experimental rack, 6: Electric furnace controller, 7: High speed data logger, 8:Data logger, 9:PC, 10:Turbine flow meter, 11:FV converter, 12:Ice box, 13:Feed water pump, 14:Spray nozzles, 15:Jet pump, 16: Ring header of spray nozzles, 17:Cold bath, 18:Water heater

Fig.1 Schematic of experimental apparatus

suspended at the center of the ring header. Spray jets were overlapped around the specimen. The spray nozzles for N = 4 and 8 were fixed at mounting angle θ of 0 deg (horizontal) and 23 deg to get uniform spray impingements under the constraint of the nozzle layout in the quench bath. Two different flow capacity full-cone spray nozzles were used for four and eight sprays quenching. Due to the limitation of the feed water pump capacity, total spray flow rate impinged from the nozzles were below 20 L/min. Therefore, liquid flow rate per nozzle for the 4 nozzles layout was about twice as large as that for the 8 nozzles layout. However, overlap area on the outer surface of the specimen with 8 spray impingements became greater than that with 4 spray impingements. More uniform spray impingements around the outer surface were obtained with the 8 nozzles set-up.
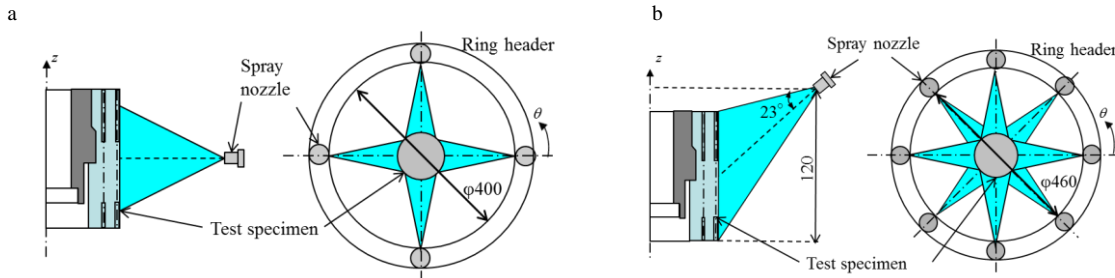
Fig.2 Layout of the spray nozzles and test specimen (Top and side views) (a) 4 spray jets impingement (b) 8 spray jet impingement.

2.2. Test specimen

Figures 3 (a) and (b) show cross sectional side view and top view for two types of test specimens. Each specimen was a part of nozzle which was cut away from an end of a Type-III aluminum pressure vessel liner for high pressure (35 MPa) hydrogen vessel. The vessel liner was made of aluminum alloy A6061 by spinning foaming machining. The test specimen was a thick A6061 hollow cylinder and it had a stainless steel SUS316 hollow cylinder part inside. The specimens for N = 4 and 8 were quite similar except for angular positions of thermocouple wells. A pair of the two radial positions of the wells at each level of z was aligned to the spray nozzle or a center of the nozzles (θ = 45 deg for N = 4 and 22.5 deg for N = 8) to evaluate the circumferential distribution of cooling rate. Thermocouple wells of φ1.1 mm were made in the specimen by electric discharge machining. A grounded K-type sheath thermocouple (φ1 mm) was inserted into each well. Inside temperature of the test specimen was measured at the two height levels of z = 15, 64 mm. Temperature and heat flux distributions in radial direction at each level were evaluated by the 1D inverse heat conduction analysis technique proposed by the authors [5]. The inverse analysis technique was based on analytical method with the Laplace transform technique and not used numerical analysis such as well-known conjugate gradient methods. Both ends of the test specimen were covered with caps not to contact with water during quenching process.

2.3. Experimental procedure

T6 heat treatment of A6061 consists of three processes such as solution treatment, quenching and artificial aging.
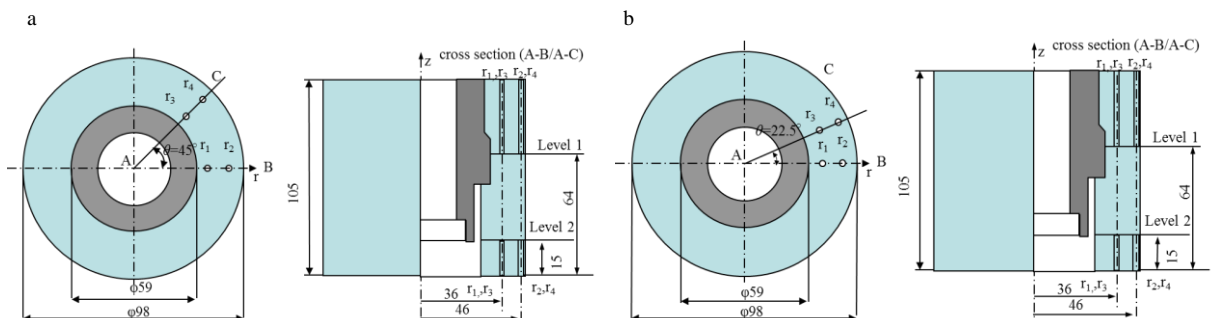
Fig. 3 Cross sectional side view and top view of the cylindrical specimen (a) 4 spray jets impingement   (b) 8 spray jets impingement.

In solution process the test specimen kept at 535 ºC for 21 minutes in the electric furnace. Then the test specimen was brought out and transferred to the quenching bath equipped spray nozzles. The coolant water temperature was at room temperature. In dip (bath) quenching, the specimen was quickly soaked into water. In spray quenching, the specimen was fixed at the prescribed position in the quenching bath given in Fig. 2. Then the quenching was started by switching on the feed water pump. Cooling of the specimen was stopped when the specimen temperature readings reached at the liquid temperature. Since a long time was required to cool the electric furnace to the artificial aging temperature of 171 ºC, the test specimen was stored in the cold bath at -15 ºC to prevent the specimen from progress in aging at room temperature. The test specimen was transferred from the low temperature bath to the furnace of 171 ºC. The specimen was kept for 8 hrs after the specimen temperature reached at 171 ºC. After finishing the aging process, the specimen was cooled down to room temperature in the furnace. The specimen temperatures, cooling water and feed water flow with time were recorded in the PC during the quenching. After experiments, the surface temperature and the internal temperature distribution change were estimated with the 1D inverse heat conduction analysis at each vertical level in the specimen.

The experimental range for the dip quench and the spray jet quench are listed in Table 1. The dip quenching test was done only at water temperature of 18 ºC. This test was a reference to estimate potential of spray quenching. In spray quenching, the test specimen was quenched with four or eight spray nozzles under the water temperature range from 10 ºC to 20 ºC. The total spray flow rate was below 20 L/min due to limited performance of the feed water pump.

Table 1 Quenching condition

Quenching method	Dip quench	Spray quench	
		4	8
Number of spray nozzles N	N/A	4	8
Liquid temperature T_l, ºC	18	12.7, 22	10, 20
Total spray flow rate Q_{spray}, L/min	N/A	18.2, 20.5	7.9, 16.5

2.4. Material strength tests

Material strength tests with the strip specimens were done for T6 heat treated test specimens to evaluate sensitivity of cooling rate during quenching on the strength such as ultimate tensile stress (UTS) and elongation. The strip specimens of 2.5 mm thickness were cut away from the locations of the cylindrical specimen as shown in Fig.4. The dimension of the tensile specimen is given in Fig. 5. The strip specimens were taken along the two direction lines denoted as A and B in Fig. 4 which oriented to the spray nozzle and the intermediate between the spray nozzles, respectively. Tensile tests were conducted by a universal tensile testing machine. Elongation of the strip between the gauge lines was measured by a non-contact camera extensometer. The temperature histories suffered by the strip specimens were estimated by the 1D inverse heat conduction analysis based on the measured temperature changes at the two radial positions (denoted as the open circles) on the corresponding direction line to the direction of A or B.
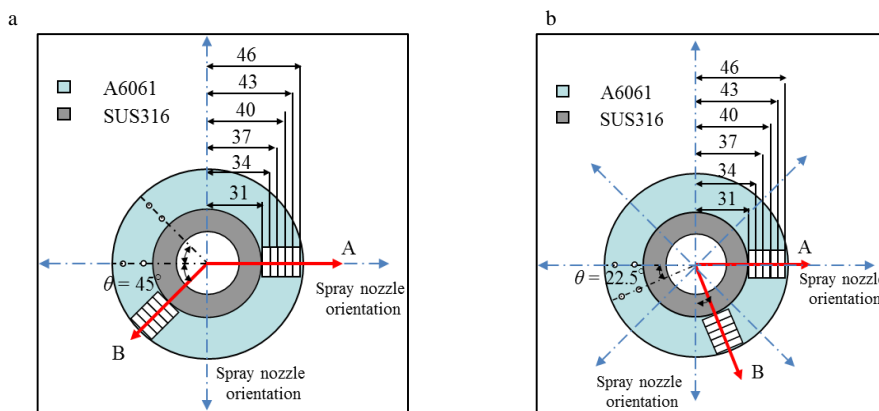
Fig. 4 Location of strip tensile specimen cutting from the cylindrical specimen (φ98mm) (a) Four spray nozzles (b) Eight spray nozzles
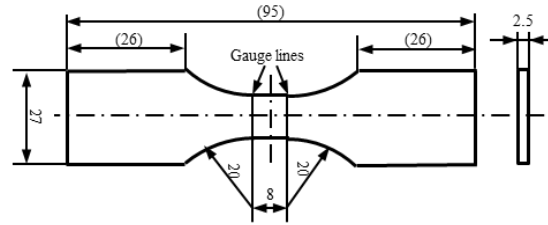
Fig. 5 Dimension of a strip tensile specimen

3. Experimental results and discussions

3.1. Cooling temperature history during dip quenching

Figures 6(a) and (b) show cooling temperature histories in the test piece during the dip (bath) quenching which is commonly used. The temperatures were measured at $z = 54$ mm. Figures 6 (a) and (b) show the history for entire range of time and for the range of our interest from 0 to 30 s. In Fig.6(b) straight lines drawn on the cooling curves measured at $r = 31.5$ and 45.5 mm indicate change in cooling rate before and after quenching at 5.1 s. Cooling curves were also categorized into four regions denoted as A, B, C and D. These time regions were decided by change in cooling rate based on visual observation and change in boiling sound. The features of the regions are as follow. For the dip quenching the maximum delay time of 5.1 s when the inside temperature reached at 360 ℃ was recorded.

Region A: Moderate cooling rate from -21 K/s to -33 K/s in the specimen were indicated. Film boiling was dominant

Region B: Sudden increase in cooling rate was recorded. Large cooling rate from -36.7 K/s to -142.8 K/s were recorded as the radial position goes outside due to recovery of surface wetting and violent nucleate boiling.

Region C: Single phase natural convective heat transfer was dominant. This region was characterized by constant temperature distribution due to balance of heat supply from the inside SUS-316 cylinder and cooling heat transfer.

Region D: The temperature kept uniform radial temperature distribution and gradually decreases with time. Then the temperature approached to the coolant temperature. The fact of the uniform temperature distribution implies the Biot number reduces below 0.1 due to poor natural heat transfer.
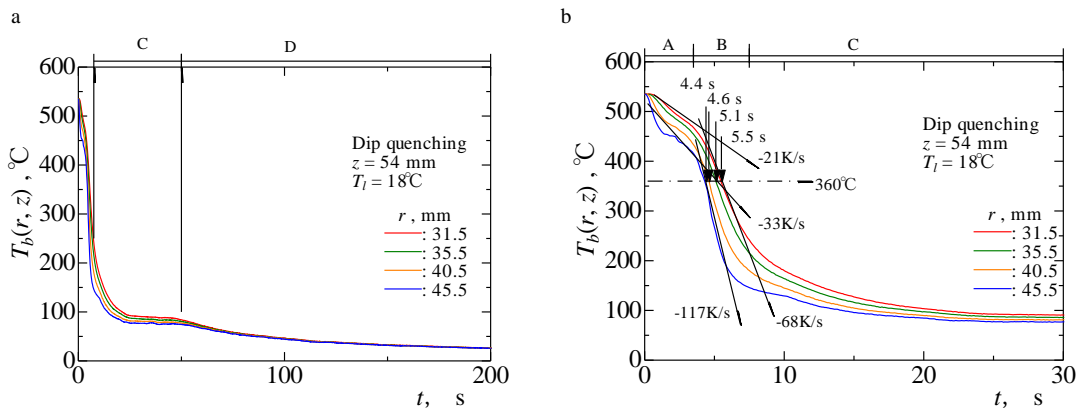
Fig. 6 Cooling temperature histories in the cylindrical test specimen during dip quenching (a) entire time range (b) close-up time range

3.2. Cooling temperature histories during spray quenching with different spray nozzle layouts

Figure7 shows the temperature histories T_b measured in the specimen during the spray quenching with 4 spray nozzles. Figure 7 (a) denotes comparison of T_b at different radial and angular positions. Figure 7(b) also indicates the comparison of the cooling curves at two different liquid temperatures of $T_l = 11.5$ and 21.5 ℃. As shown in Fig.6, the

temperature histories were categorized with the regions of A-D, and quenching delay time was denoted with arrow on each history. For reference, the cooling curve of the dip quenching was depicted with the blue line.

In Fig.7 (a) the temperature difference at $r = 36$ and 46 mm in the direction of $\theta = 0$ deg was larger than that in $\theta = 45$ deg. During the region of A, the temperature difference at $\theta = 0$ deg reached at 80K, but that at $\theta = 45$ deg indicated smaller difference of about 10 K. The radial heat transfer rate with heat conduction showed maximum just beneath the spray nozzle where highest impingement pressure was indicated. The spray quenching delay times reaching at 360 ºC ranged from 6.6 s to 12.2 s which was longer than 5.1 s for the dip quenching. In Fig.7 (b) T_b for the two different liquid temperatures of $T_l = 11.5$ and 21.5 ºC are similar with Fig.7 (a). However, lower spray temperature condition resulted in shorter quenching delay time. The delay time at lowest water temperature $T_l = 11.5$ ºC was within 12 s but it delayed about 7 s for the dip quenching result. The quenching delay time t_{d360} for $z = 15$ and 64 mm agreed within 1 s at the same radial position regardless of angular direction and liquid temperature. Vertical location z appears to have minor effect on the cooling rate.

Figure 8 shows the measured temperature histories T_b during the spray quenching with 8 spray nozzles. Figure 8(a) depicts T_b at different r and θ for the spray cooling condition of $Q_{spray} = 16.5$ L/min and $T_l = 20$ ºC. The differences between T_b at the different measurement positions became considerably small as compared with Fig.7 for $N = 4$. Spray impingement areas were overlapped more on the outer surface of the specimen so that uniform cooling was recorded. However, spray flow rate of each nozzle reduced due to the limitation of the maximum Q_{spray}, namely uniformly spray cooling was achieved as increasing in spray nozzle number. Therefore, quenching delay time for $N = 8$ indicated about two times longer than that for $N = 4$. Figure 8(b) denotes the comparison of T_b for $Q_{spray} = 7.9$ and 16.5 L/min, $N = 8$ and $T_l = 20$ ºC. At the lowest spray flow rate $Q_{spray} = 7.9$ L/min, quite uniform temperature histories and longest delay time of 75 s were recorded regardless of z and θ directions. Because quenching hardly started until T_b at $r = 46$ mm reached at 280 ºC. The other condition the quenching started above 300ºC.

The facts explained above tell us that uniform cooling in the specimen and short quenching delay time are incompatible. Uniform cooling in circumferential direction was obtained with 8 spray nozzles. Spray quenching with 4 nozzles at $T_l = 11.5$ ºC and $Q_{spray} = 17.8$ L/min has a potential to cool the specimen from 536ºC to 360ºC within the allowable quenching delay time of 10 s which is expected by Ref. [1]. Due to a limit of the present feed water pump capacity, the spray quenching with 8 nozzles required the quenching delay time of 24 s. Therefore, it is found that larger spray flow rate than 16.5 L/min is required for 8 sprays quenching at $T_l = 20$ ºC.

3.3. Assessment of quenching delay time during spray quenching with inverse heat conduction analysis

Figures 9 and 10 show the typical results of the inverse analysis for N= 4 and 8, and $z = 64$ mm. The black solid lines denote histories of estimated cooling temperature T_b at each inner radial position, and the red and blue solid lines are the estimated inner and outer surface temperatures of $T_w(R_i)$ and $T_w(R_o)$. The dashed red and blue lines give radial
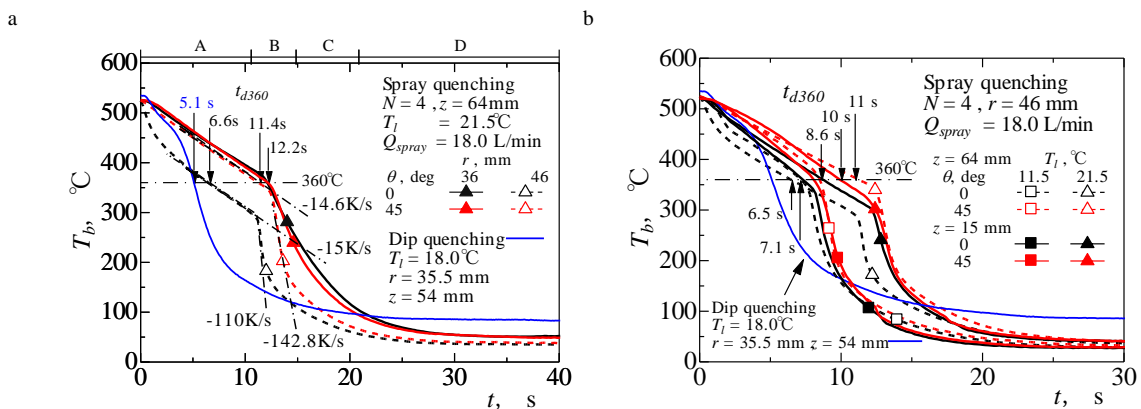
Fig. 7 Cooling temperature histories measured in the cylindrical specimen during spray quenching for $N = 4$, (a) effect of radial and angular positions at $z = 64$ mm, $T_l = 21.5$ ºC and $Q_{spray} = 18.0$ L/min, (b) effect of spray water temperature on cooling temperature histories measured in the cylindrical specimen at $z = 15$, 64 mm and $Q_{spray} = 17.8$ L/min.

transferred heat rate per unit axial length of $q_w'(R_i)$ and $q_w'(R_o)$ on the inner and outer surfaces, respectively. q_w' was calculated by the product of the local heat flux and the perimeter of $2\pi R_i$ or $2\pi R_o$. The inverse solution was evaluated for each angular direction at $z = 64$ mm as shown in Fig.3.

In Fig.9(a) T_w and q_w' on the outer surface were categorized into four regions denoted as I – IV corresponding to measured temperature changes denoted as the regions of A-D in Fig.7(a). From change in the radial transmission rate q_w' and observation, we can see the following characteristic of each region.

Region I: $q_w'(R_o)$ recorded a constant value of 0.6 MW/m and the heat transmission to the A6061 hollow cylinder from the SUS316 also kept 0.3 MW/m. Thus constant temperature cooling rate inside the specimen indicated. According to the visual observation and boiling sound, film boiling heat transfer was dominant on the outer surface.

Region II: Surface wetting situation was quickly recovered and the boiling situation shifted from film boiling to transition boiling on the outer surface to be accompanied by vigorous boiling sound and steam generation. The heat transfer rate on the outer surface $q_w'(R_o)$ suddenly increased and recorded the maximum value of 1.5 MW/m. Thus sudden drop in the outer surface temperature started to propagate into the hollow aluminum cylinder.

Region III: The boiling sound gradually calmed down as the outer surface heat transfer rate $q_w'(R_o)$ quickly decreased and the surface temperature approached to the saturation temperature of 100 ℃. The maximum surface cooling rate was recorded just after the inception of the region III.

Region IV: The outer surface temperature became below 100 ℃ and the heat transfer mode on the outer surface shifted to single phase convective heat transfer. The outer heat transfer rate $q_w'(R_o)$ gradually decreased and approached to $q_w'(R_i)$ with time. Thus temperature at each inside location reached to steady state.
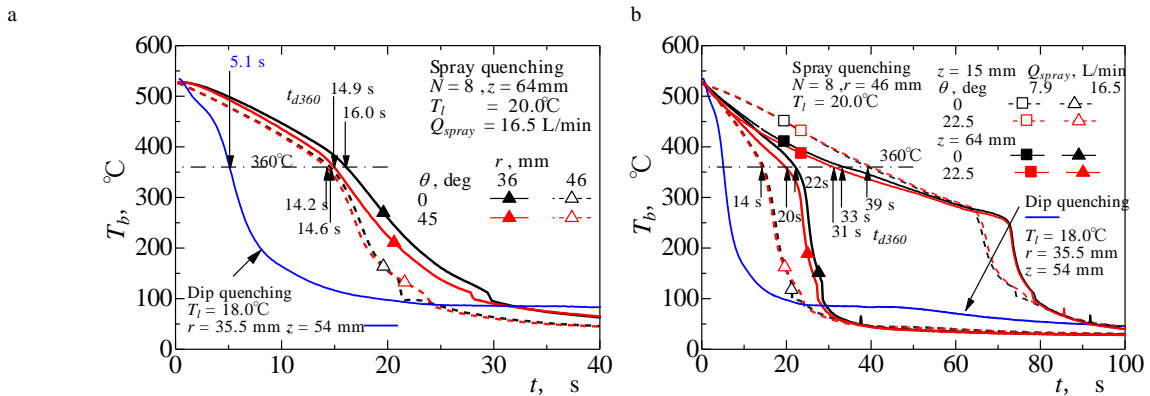
Fig. 8 Cooling temperature histories measured in the cylindrical specimen during spray quenching with 8 nozzles ($N = 8$) (a) effect of radial and angular positions at $z = 64$ mm, (b) effect of spray flow rate at $r = 46$ mm.
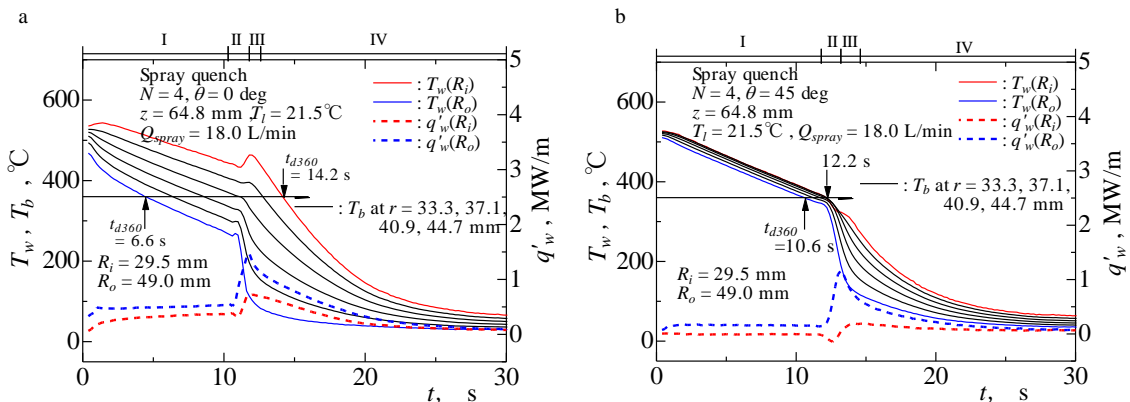
Fig. 9 Results of inverse analysis for spray quenching with 4 nozzles at $Q_{spray} = 18$ L/min and $T_l = 21.5$ ℃ (a) $\theta = 0$ deg , (b) $\theta = 45$ deg

In case of N =4, surface temperature decreased quickly and large temperature gradient due to strong cooling just beneath the spray nozzles (θ = 0 deg) was shown. t_{d360} on the outer surface was considerably changed in the radial direction. However, t_{d360} at inner surface r =R_i indicated 14.2 s and 12.2 s for θ = 0 deg and 45 deg. On contrary of this, t_{d360} for N = 8 were hardly changed with the angular direction and radial position but those were longer than t_{d360} for N = 4. From Figs.9 and 10, the spray nozzles number of eight is better to get uniform cooling history in the specimen. Quenching with four nozzles can accelerate cooling rate of the specimen only adjacent to the outer surface beneath the nozzles. However, quenching delay time of the inner position was hardly affected so much with number of nozzle at the same total spray flow rate.
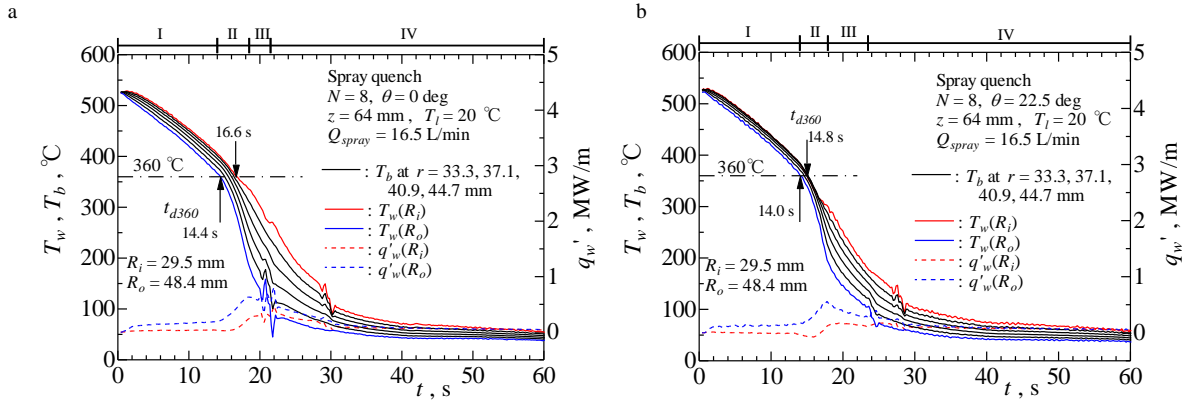
Fig. 10 Results of inverse analysis for spray quenching with 8 nozzles at Q_{spray}= 16.5 L/min and T_l = 20 ºC   (a) θ = 0 deg , (b) θ = 22.5 deg

3.4. Effect of quenching delay time on mechanical strength of specimen

Relationships between the ultimate tensile stress (UTS) σ_B and the quenching delay time t_{d360} for the spray quenched tensile strip specimens with 4 and 8 nozzles are shown in Figs. 11 and 12. t_{d360} was decided from the estimated temperature change at radial position of the center of each strip specimen with the inverse heat conduction analysis. For reference, the results of the dip quenched strip specimens were also denoted with blue open circle symbols which indicate from 320 to 350 MPa. Solid red and open red symbols denoted UTS data of spray quenched specimens cut from the angular directions of A and B shown in Fig.4. The UTS of Aluminum alloy A6061-T6 for pressure vessels is specified the minimum UTS of 310 MPa in JIS (Japanese Industrial Standards) B8270 and it is depicted as a dot-dash line in Figs.11 and 12. the UTS for the dip quenched specimens.
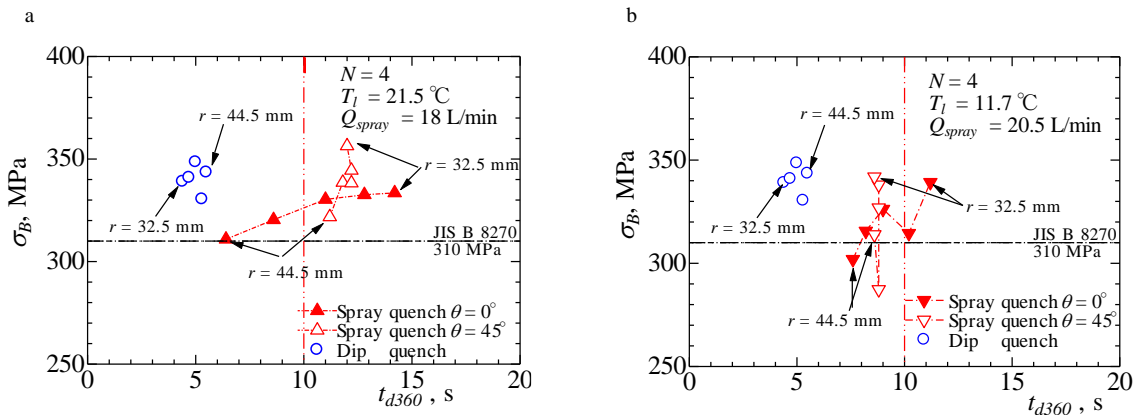
Fig. 11 Relationships between ultimate tensile stress and quenching delay time reached at 360ºC for quenching with 4 spray nozzles.
(a) T_l = 21.5ºC, Q_{spray} = 18 L/min (b) T_l = 11.7 ºC, Q_{spray} = 20.5 L/min
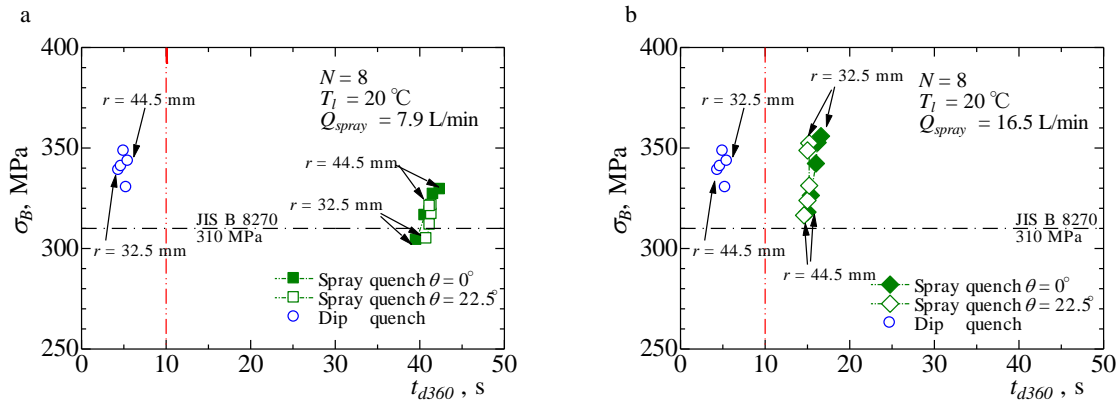
Fig. 12 Relationships between ultimate tensile stress and quenching delay time reached at 360 ºC for quenching with 8 spray nozzles.
(a) T_l = 20 ºC, Q_{spray} = 7.9 L/min (b) T_l = 20 ºC, Q_{spray} = 16.5 L/min

Remarkable results in Figs.11 and 12 are as follows. 1) Even though the delay time t_{360} was beyond the allowable delay time of 10 s, the UTS did not show apparent decrease with increase in t_{360}.and most of UTSs satisfied the minimum UTS. But the spray quenched specimens indicated larger standard deviation than that for the dip quenched specimens. 2) the UTSs of the spray quenched specimens which were subjected to much longer delay time t_{360} = 40 s, indicated from 300 to 330 MPa contrary to the expectation of Ref. [1].

4. Conclusions

Application of spray quenching to T6 thermal treatment of the aluminum A6061 thick hollow cylinder specimens cutting from the Type-III high pressure vessel liner has been considered with assessments of the local cooling temperature delay time and tensile strength test of the strip specimens. From the spray quench test under the conditions of the total spray flow rate up to 20 L/min and spray nozzles number of 4 and 8, and water temperature from 10 to 20 ºC, it was confirmed that the spray quenching delay time at 360 ºC can achieve within 16.6 s. However, the quenching time was longer than typical delay time of 5 s for the conventional dip quenching. The experimental results showed that uniform spray cooling temperature distribution in the specimen and short quenching delay time were incompatible. The UTSs of the spray quenched strip specimens were independent of quenching delay time within 16.6 s and most of them satisfied the minimum UTS of 310 MPa prescribed with the code and standard.

References

[1] S. C. Bergsma, M. E. Kassner, X. Li, and R. S. Rosen, The Quench Sensitivity of Hot Extruded 6061-T6 and 6069-T6 Aluminum Alloys, Proc. 3ed Int. Conf. on Processing and Manufacturing of Advanced Materials (in CD-ROM), (2000).
[2] David Hall, Issam Mudawar, Experimental and numerical study of quenching complex-shaped metallic alloys with multiple, overlapping sprays, Int. J. Heat and Mass Transfer, 38 (1995) 1201-1216.
[3] Nikhin Mascarenhas, Issam Mudawar, Analytical and computational methodology for modeling spray quenching of solid alloy cylinders, Int. J. Heat and Mass Trans., 53(2010) 5871–5883.
[4] Nikhin Mascarenhas, Issam Mudawar, Methodology for predicting spray quenching of thick-walled metal alloy tubes, Int. J. Heat and Mass Transfer, 55 (2012) 2953-2964.
[5] H. Arima, M. Monde and Y. Mitsutake, Estimation of Surface Temperature and Heat Flux using Inverse Solution for One Dimensional Heat Conduction, Thermal Sc. and Eng., 10 (2002) 27-37.

6th BSME International Conference on Thermal Engineering (ICTE 2014)

Characteristics of transient heat transfer and wetting phenomena during laminar jet quenching on rotating cylinder

Shinya Tsuboyama[a], [a]Tomofumi Higashi[a], Yuichi Mitsutake[b]*, Suhaimi bin Illias[a], Aloke Kumar Mazumder[c], Koutaro Tsubaki[a] and Masanori Monde[d]

[a]*Graduate school of Science and Technology, Saga Univerdity, 1 Honjo-machi, Saga-shi, Saga 840-8502, Japan*
[b]*Institute of Ocean Engergy, Saga Univerdity, 1 Honjo-machi, Saga-shi, Saga 840-8502, Japan*
[c]*Department of Mechanical Engineering, Bangladesh University of Engineering & Technology, Dhaka 1000, Bangladesh*
[d]*International Research Center for Hydrogen Energy, Kyushu University, 744 Motooka, Nishi-ku, Fukuoka-shi, Fukuoka, 819-0935, Japan*

Abstract

Hot strip leaving from finishing roll is quenched from about 850 to 500 degC by array of laminar jets on cooling table (Run-Out-Table). Cooling temperature control of the hot strip is important to obtain better mechanical strength and grain size. However, the cooling process includes unstable transition boiling region as well as moving boundary problem due to relative movement between the hot strip and the jets. To improve quality of hot strip deeper understanding about laminar jet quenching process on the moving hot surface should be elucidated. In this study, single laminar jet quenching tests on a rotating hollow hot cylinder mounted horizontally have been conducted to understand characteristics of transient heat transfer and wetting phenomena. The experiments were done for 18-8 stainless steel (SUS304) hollow cylinder (O.D. 136mm, I.D. 116mm, W 150mm) under rotational speed ranged from 15 to 60 rpm, cooling water temperature ranged from 10 to 60 ºC (corresponding degree of subcooling 40-90 K) and flow rate ranged from 6 to 23 L/min. Surface temperature and surface heat flux on the rotating cylinder were estimated from two sheath thermocouples embedded at two depths from the outer surface with one dimensional inverse heat conduction analysis. Visual observations over the top surface were done with two normal speed video cameras which were synchronized with rotating cylinder temperature recording. The observation results show that unstable wetted area was gradually growing from the stagnation area and finally the wetted area became continuous around the circumference of the cylinder. It was found that the growth and shape of the wetted area were strongly affected by the liquid temperature and the liquid flow rate. Wetted front which is the boundary between wetted and dry areas repeated advance and recession. Since the wetting area propagated faster in the rotational direction, the shape of the wetted area was asymmetry on the hot surface. The liquid film flow was completely splashed out due to violent nucleate boiling on the wetted front line. The characteristics of local transient heat transfer were evaluated with boiling curves taken around the stagnation point. The boiling curves indicated shift to much higher wall superheat as compared with a steady state pool boiling

---

* Corresponding author. Tel.: +81-952-28-8616; fax: +81-952-28-8587.
  E-mail address: mitutake@me.saga-u.ac.jp

curve and those were categorized into three regions such as 1) single phase heat transfer, boiling heat transfer and 3) transition boiling by inspecting gradient of the boiling curves and the observation of the boiling situations. The transition boiling region disappeared and the single phase heat transfer became dominant for higher subcooling and higher flow rate conditions.

1. Introduction

Steel manufacturing industries are trying to improve thermomechanical treatment process to product high value added hot strips such as high tensile stress (HTS) steel, dual phase (DP) steel and transformation induced plasticity (TRIP) steel. In order to reduce adding expensive metal elements like nickel or manganese to carbon steel, precise temperature control of low alloy steel strips over entire of width and length attracts great interest to produce such high value added steels. In case of the TRIP carbon steel production process, hot strip at about 800°C is quenched to about 400 °C with laminar or spray jets impingement on run-out-table (ROT) after finishing roll. To ensure mechanical properties, controlled cooling of the strips is required a severe allowance error in final temperature within 20 K. Though state of art control technology such as learning or predictive controls is applied to online control of strip temperature at the exit of the ROT, accuracy of temperature control and process yield still do not reach to a satisfactory level. Especially when the target strip temperature is in the transition boiling region empirically known as 500-550 °C in steel manufacturing industries, control of the hot strip temperature becomes difficult due to the termination of cooling at very unstable transition boiling region. In the transition boiling, boiling situation changes from film boiling to nucleate boiling due to recovery of wetting on hot surface. Since the surface heat transfer coefficients dramatically change whether the surface is wetted or not, the temperature control faces with a difficulty. Rewetting phenomenon is also known to be very sensible to surface conditions such as surface roughness, thickness of poor heat conductive oxidization layer as well as coolant conditions as water temperature and intensity of liquid momentum impinged on a hot surface. Despite of many studies and challenges to understand the transient transition boiling heat transfer and the wetting process on hot surface, a lot of elementary processes about this phenomenon are still remained for us.

Recently considerable studies on quenching hot surface at high initial temperature up to 800-900 °C with pipe laminar, slit laminar and spray jets were reported and characteristics of transient transition boiling heat transfer were elucidate to understand elementary process from film to transition boilings, namely rewetting process. However, thin strip of a couple of millimeters in thickness is quenched during transfer on ROT at maximum velocity of 60 km/h. Thus quenching process of the strips becomes moving heat sink boundary problem. However, reproduce of similar experiments with real processes are very difficult in a laboratory. Most of existing experimental studies were done for stationery heated surface and experiments with moving surface are limited as far as the authors know.

For example, Gradeck, et al. [1] conducted experimental study on boiling heat transfer during quenching of rotating hot hollow cylinder with slit laminar jet. Quenching heat transfer distributions were obtained for different rotational speed by using boiling curves. Aloke, et al. [2] also reported experimental study on laminar jet quenching on rotating hollow cylinder as our previous study. Characteristics of non-uniform wetting front propagation which is identified as the location at leading edge of the wetted area, and comparison of maximum heat flux with steady state critical heat flux were elucidated at two rotational speeds and different flow rates and coolant water temperatures.

In this study we conducted the experiments using the previous experimental apparatus [2] over the extensive experimental range of coolant water temperature, laminar flow rate and rotational speed. Image analysis of boiling video provided the characteristic of rewetting process on the moving hot surface. Surface temperature and surface heat flux on the outer surface were evaluated with one dimensional inverse heat conduction analysis. Effects of circumferential positon, coolant water temperature, laminar flow rate and rotational speed on boiling curve were elucidated in particular.

Nomenclature

a	thermal diffusivity (m²/s)
d_j	inner diameter of the laminar jet nozzle (m)
N	rotational speed of cylinder (rpm)
q_w	surface heat flux (W/m²)
Q	volumetric flow rate of laminar jet (L/min)
r	radial coordinate (mm)
S	circumferential coordinate of curvilinear coordinates system on outer surface of the cylinder (mm)
t	time (s)
$t_{wet,i}$	time when the stable wetting area was formed at the stagnation point (s)
$t_{wet,f}$	time when the circumferentially continuous wetting area was formed around the cylinder (s)
T_b	measured temperature in the cylinder wall (°C)
T_{bo}	initial temperature of the cylinder (°C)
T_l	laminar water jet temperature (°C)
T_w	surface temperature (°C)
W_s	characteristic dimension of wetting front distribution in circumferential direction (mm) (See Fig.4(b))
W_x	characteristic dimension of wetting front distribution in axial direction (mm) (See Fig.4(b))
X	axial coordinate of curvilinear coordinates system on outer surface of the cylinder (mm)
y	depth from the outer surface (mm)
z	axial coordinate (mm)

Greek letters

ΔT_{sat}	wall superheat (K)
ΔT_{sub}	degree of liquid subcooling (K)
λ	thermal conductivity (W/m/K)
θ	angular position of thermocouple (rad)

2. Experimental apparatus and procedure

2.1. Experimental apparatus

The schematic of the experimental apparatus is shown in Fig.1. A rotating hollow cylinder mounted horizontally was quenched by a downward single laminar water jet. The water supply system circulated water between the bottom and upper tanks of total capacity 350 L with a feed water pump and controlled water at designated temperature up to 60 ºC with by total 16 kW heaters equipped with the tanks. The water was supplied to the nozzle at a constant water head from the upper overhead tank. The laminar jet velocity was evaluated with pressure loss between the inlet and outlet of the nozzle and the flow coefficient of the nozzle calibrated by preliminary test. The test cylinder was rotated in anti-clockwise as indicated arrows in Fig.1. Two cameras took movie of wetting surface. The top of 202.2 deg range of the cylinder surface was observed with the two cameras. Start time of the two cameras were synchronized with the data acquisition system.

Figure 2 shows dimension of the tested hollow cylinder and locations of thermocouples embedded in the cylinder wall. The test cylinder was 150 mm in length, 136 mm in outer diameter and 116 mm in inner diameter. Material of the test cylinder was SUS304 which has no phase transition point over the experimental temperature range from 10 ºC to 900 ºC. The grounded K-type sheath thermocouples of O.D. 1 mm were embedded at the axial center position at the two different depths of 1.5 and 3.5 mm from the outer surface. Two pairs of the two different radially located thermocouples were directed to the two angular directions of $\theta = 0$ and π as shown in Fig.2. Surface temperature and surface heat flux were evaluated with the one-dimensional transient inverse heat conduction analysis proposed by the authors [3] from measured temperature histories. The hollow cylinder was heated to initial temperature in an electric furnace and it was mounted horizontally on the test bench as shown in Fig.3. The test cylinder was rotated with a pulse motor drive unit at a designated rotational speed. Thermal electromotive force signals from the thermocouples were

transmitted to an instrumental apparatus via 8ch mercury rotary contactors. The test bench was mounted on the bottom tank so that the axially center point of the cylinder was adjusted to the stagnation point of the laminar jet.

2.2. Experimental condition and procedure

The present experiments have been done by changing in the rotational speed N, the water temperature T_l (liquid subcooling ΔT_{sub}) and the laminar jet flow rate Q as the experimental parameters. The range of these parameters is tabulated in Table. 1. The rotational speed of the cylinder was decided by the similarity of the thick hollow cylinder wall with thin hot strip. For example, ratio of Fourier numbers for 1 mm of low carbon steel wall ($a = 1.4 \times 10^{-5}$ m^2/s) and 10 mm of stainless steel SUS304 ($a = 4.01 \times 10^{-6}$ m^2/s) becomes about 350. That means that the stainless temperature changes at about 350 times slower than that of the low carbon steel. Therefore, circumferential velocity of the stainless steel hollow cylinder at $N = 15$ rpm corresponds to the equivalent moving velocity of 67 km/h for the low carbon steel. A large time scale factor between the tested hollow cylinder and thin strip brings advantages to designing the experimental apparatus and making measurement of transient temperature in the wall easier in laboratory tests. Thus we selected the rotational speeds from 15 to 60 rpm which corresponds to the real hot strip transfer velocity.

The storage water was heated at experimental liquid subcooling during water circulation between the tanks. During heating feed water, opening of the flow control valve was previously adjusted to the designated liquid flow rate. To prevent the laminar water jet from impinging on the hot test cylinder before starting experiment, water supply to the laminar nozzle was bypassed to the bottom tank through a three-side cock.
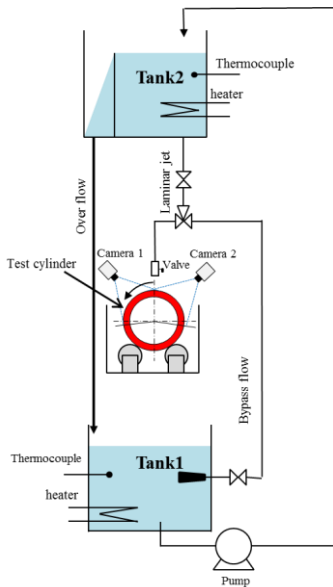
Fig.1 Experimental apparatus (feed water system)
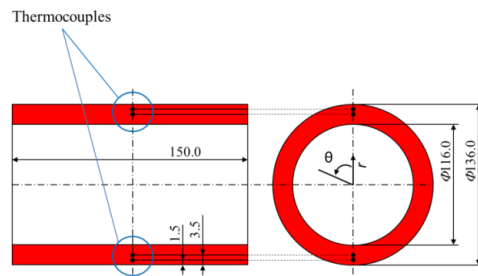
Fig.2 Dimension of the test cylinder and locations of thermocouples
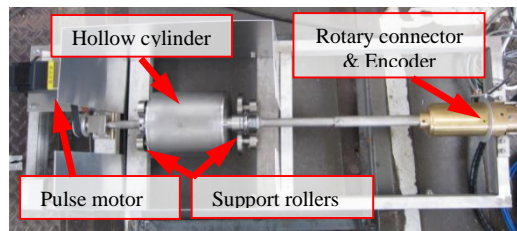
Fig.3 Top view of the test bench

Table 1 Experimental range.

Inner diameter of laminar nozzle d_j [mm]	15
Subcooling of Water ΔT_{sub} [K]	50, 60, 70, 80, 90
Flow rate of laminar jet Q [L/min]	6, 10, 15, 23
Impinging jet velocity u_j [m/s]	1.3, 1.6, 2.0, 2.8
Initial temperature of cylinder T_{bo} [ºC]	780 – 805
Rotational speed of cylinder N [rpm]	15, 20, 30, 60
circumferential speed of outer cylinder surface v_θ [m/s]	0.11, 0.14, 0.21, 0.42

The test cylinder being suspended in a crucible electric furnace was heated to up to 870 ºC. Then, the test cylinder was got out and mounted on the test bench and then transferred just beneath the laminar jet nozzle as soon as possible until starting quenching. The motor drive system was switched on and the data acquisition system and the two video cameras (30 fps) were triggered to start recording by the rotary encoder. The trigger signal is synchronized with the rotational angle of the thermocouples precisely. Then the three-side cock was turned to start laminar jet quenching. The video cameras recorded change in boiling situation on the upper half of the rotating cylinder surface. The laminar jet impingement ceased until wetted area continuously covered around the circumference of the cylinder surface.

3. Experimental results and discussion

3.1. Visual observation of boiling situation during quenching of rotation hollow cylinder

Typical boiling situation on the rotating cylinder at elapsed time of 14 s after starting laminar jet quenching was shown in Fig.4. The corresponding experimental condition was for the rotational speed of $N = 60$ rpm, the liquid subcooling of $\Delta T_{sub} = 70$ K and the flow rate of $Q = 10$ L/min. The rotational direction of the test cylinder was denoted with the yellow arrow. Stagnation point of the laminar jet on the hot surface was indicated with the white dot and the arrow. A black area distributing around the stagnation point was covered with single phase liquid film (S.P.F.) and steady liquid-solid contact and single phase convective heat transfer were observed but net bubble nucleation was invisible. The outer boundary of S.P.F. denoted with the blue dashed line agreed with the onset of nucleate boiling (O.N.B.) locations beyond which violent nucleate boiling (N.B.) took place. The nucleate boiling region was visible as bright (white) zone in the photo, and the region size was ranged from a few millimeters to tens of millimeters depending on the direction from the stagnation point. On the downstream of the S.P.F. area just behind the O.N.B., subcooled boiling (S.B.) area accompanied weak surface boiling was also observed. The liquid film flow along the surface was completely splashed out as droplets at the outer edge of the N.B. region and the hot surface was dry on the hot surface outside of the N.B. region. The boundary between the dry and the nucleate boiling regions, namely the leading edge of the wetting area denoted as the wetting front (W.F.) and it specifies wetted area on which the major cooling heat transfer occurs. Therefore, we have a great interest in growth of W.F. during laminar jet quenching and retrieved change in locus of W.F. with time by image processing of boiling videos. Figure 4(b) indicates distributions of the O.N.B. and the W.F. as the blue dashed and the red lines which were taken at elapsed time of 14 s under the same experimental condition of Fig. 4(a). The origin of Fig.4(b) was taken at the stagnation point and the longitudinal and abscissa axes were taken as the circumferential direction of S and the axial direction of X, respectively. It is noted that the negative direction of S agrees with the rotational direction. Additionally characteristic dimensions of W.F. in the circumferential and axial directions were defined as W_S and W_X in Fig.4 (b).

As shown in Figs.4 (a) and (b), the distributions of the O.N.B and W.F. indicated asymmetric in the circumferential direction and expanded faster in the rotional direction as compared with the inverse rotational and axial directions. In case of jet quenching on a stationary hot surface [4], the distributions of O.N.B and W.F. indicated concentric circles which were symmetric with respect to the stagnation point.

3.2. Change in characteristic dimensions of wetting front distribution W_s, W_x with time

Typical examples for changes in W_s and W_x of the W.F. distribution with time are shown in Figs.5(a) and (b). The experimental condition was for $N = 20$ rpm, $\Delta T_{sub} = 70$ K and $Q = 10$ L/min. The reference time of zero in the graphs was taken the time when the reference thermocouples at $\theta = 0$ passed fist beneath the stagnation point just after the jet quenching started. The definition of the reference time $t = 0$ was commonly used in showing time histories of transient data given later.

In Fig. 5(a) the locations of the both ends of W.F. in circumference direction $+W_s$ / $-W_s$ were denoted as the red and blue lines, and the characteristic circumferential length of W_s as the black line. The locations of the both ends in axial direction $+W_X$/$-W_X$ and the characteristic axial length W_X were also depicted in Fig.5(b) in the similar way. It is found that propagation of the W.F. in the circumference direction was categorized into four time regimes denoted as (a)-(d). Each photo of boiling situation taken at the corresponding to the regimes of (a)–(d) was shown in Fig.6(a)-(d),

respectively. The regime (a) with no symbols referred as "non-wetted regime" at which the laminar jet hardly contacted with the hot surface even at the stagnation point and it separated as very smooth thin liquid film flow along the surface as shown in Fig.6(a). The regime (b) referred as "unstable wetting regime" was started at about 4 s, and the location of $-W_s$ in the rotational direction gradually increased first by repeating advance and recession. However, propagation of $+W_S$ in the opposite direction was suppressed until 11 s. The W.F. was gradually advancing along the surface by repeating advance and recession. In the regime (c) after 20s denoted as "uniform advancing rate regime", surface wetting situation around the stagnation was stabilized and the wetting front monotonously and gradually advanced to the circumference direction with time. Finally the W.F. started advancing rapidly to form the circumferentially continuous wetted area around the cylinder in the regime (d) characterized with "rapid W.F. advancing regime". In contrast, constant moving velocity of the W.F. in the both axial directions of $+X/-X$ was indicated during entire the regimes in Fig. 5(b). Moving velocity of W.F. in the axial direction indicated was smaller than that in the rotational direction.

3.3. Fluctuations of internal temperatures with time

Measured typical internal temperature history at each thermocouple position with time is shown in Fig.7 (a) for the condition of $N = 20$ rpm, $T_l = 30$ ºC, $T_{b0} = 785$ ºC and $Q = 10$ L/min. The black and red solid lines show the temperature histories of $\theta = 0$ and π at the depth of 1.5 mm from the outer surface. The blue and green dotted lines are given for $\theta = 0$ and π at the depth of 3.5 mm. The symbols plotted on the lines at the interval of 3 s show the time when the

a   b
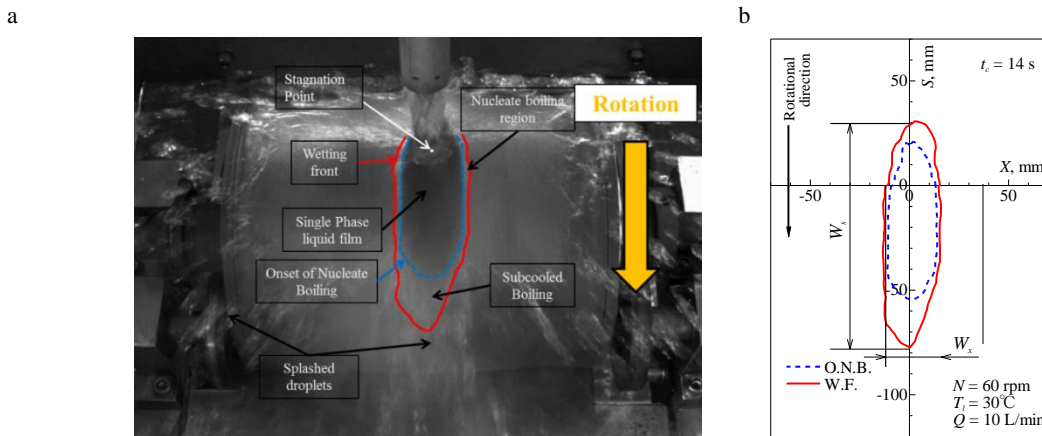
Fig.4 Definitions of flow boiling heat transfer regions, onset of nucleate boiling (O.N.B.) and wetting front (W.F.) line on the rotating hot surface. (a) Photograph of boiling situation   (b) shapes of O.N.B and W.F. lines evaluated by video image analysis

a   b
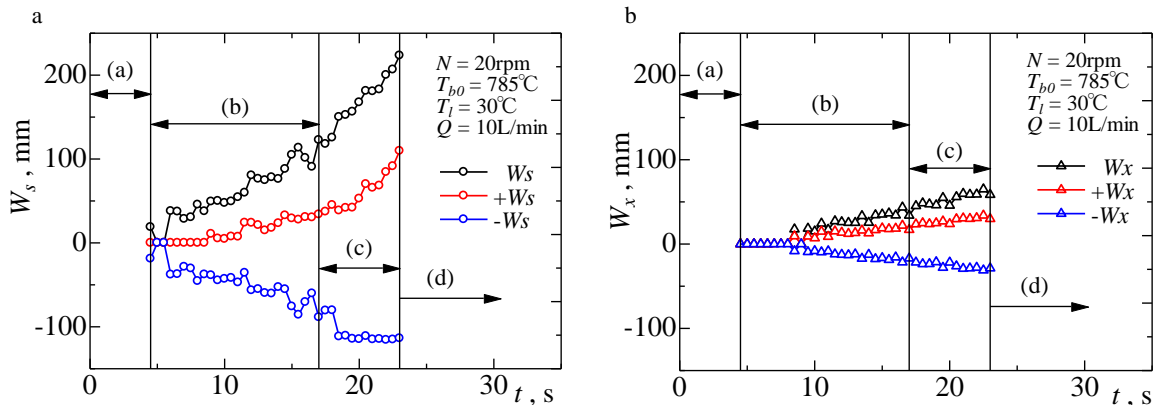
Fig.5 Change of characteristic dimensions of wetting area with time. (a) Circumferential length W_s (b) Axial length W_x
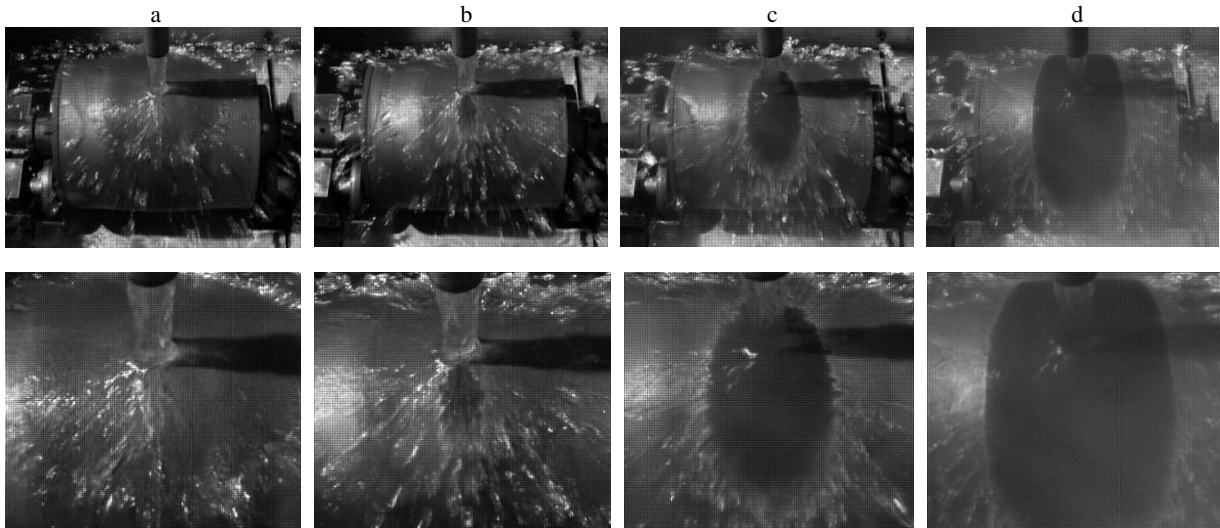
Fig.6 Photos of boiling situation on the rotor (upper side) and close-up of the stagnation area (lower side) during development of surface rewetting taken at the regimes (a) Non-wetted regime, (b) Unstable wetting regime, (c) Uniform and slow advance regime and (d) Rapid spread of wetting

thermocouple passed just below the nozzle. The arrows denoted as $t_{wet,i}$ and $t_{wet,f}$ indicate the times when the stable wetted area was observed (inception time of the regime(b)) and the circumferentially continuous wetted area was achieved on the hot surface, respectively.

It is found that the measured temperatures fluctuated at the period of 3 s in synchronization with passing beneath the stagnation point and the fluctuations at $\theta = 0$ exactly advanced as half period of 1.5 s against the fluctuations at $\theta = \pi$. These results were caused by the cooling on the wetted surface around the stagnation point and the reheating on the dry area. Noting symbols on each temperature history, we can see sudden drops at the depth of 1.5 mm started just before the thermocouple arrived at the stagnation point. The wetted area spread around the stagnation point. Amplitude of the temperature fluctuations gradually increased and indicated maximum after the inception of stable surface wetting denoted as $t_{wet,i}$. And then the amplitude decreased as repeat of the cylinder rotation and disappeared after $t_{wet,f}$ due to the continuous wetted situation around the cylinder. Meanwhile comparing temperature histories at $y = 1.5$ mm and 3.5 mm, we can see that temperature fluctuation attenuates as the radial position became deeper from the outer surface as the result of the nature of the temperature wave propagation with heat conduction in solid.
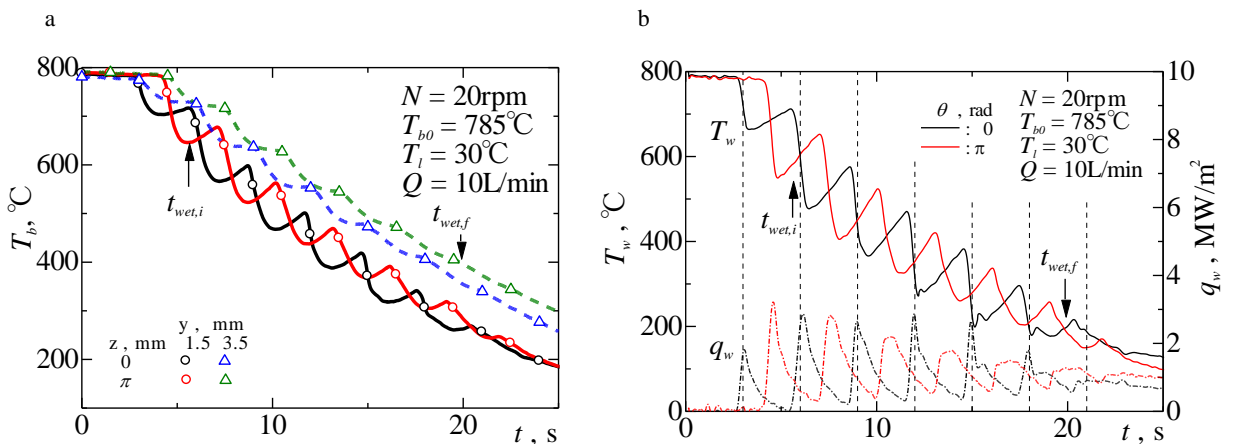
Fig.7 Measured temperature and heat flux with time for rotational speed $N = 20$rpm, laminar jet temperature $T_l = 30$ ºC and laminar flow rate $Q = 10$ L/min. (a) Temperature fluctuations during laminar jet cooling of rotating hollow cylinder, (b) Change in surface temperature and heat flux

3.4. Estimated surface temperature and surface heat flux with inverse heat conduction analysis

The surface temperature and surface heat flux were calculated by the inverse program analysis technique [3] proposed by the authors. Discussions of the evaluated surface heat transfers are given below. Typical change in surface temperature T_w and surface heat flux q_w with time is shown in Fig.7 (b). The vertical dashed lines indicate the times when the thermocouple position passed beneath the laminar nozzle. The T_w indicates very sharp drop in synchronization with passing stagnant point denoted with the dashed lines. Just after $t_{wet,i}$ drop in T_w recorded the maximum value, and then cooling duration became longer and amplitude of T_w fluctuation decreased as the rotation was repeated. The longer cooling duration was considerable after 5 periods (t = 16.5 s). The change in q_w indicated maximal value at the stagnation point. At earlier stage of the cooling, change in q_w at the stagnation point was very sharp but gradually approached to shape of plateau. The amplitude of q_w fluctuations was also decreases after $t_{wet,i}$, and disappeared after $t_{wet,f}$. The features of T_w and q_w changes shown in Fig.7(b) exactly corresponded to the visual observation of spreading wetting front in the circumferential direction after $t_{wet,i}$ due to increase in the liquid-solid contact time on the rotating measuring point.

3.5. Characteristics of boiling curve during laminar jet quenching

A typical boiling curve for the condition of N = 60 rpm, T_l = 20 ºC, T_{b0} = 776 ºC and Q = 10 L/min is shown in Fig.8. The locus of the boiling curve was depicted with the black dots and coordinates of each dot (wall superheat ΔT_{sat} and surface heat flux q_w) was retrieved at the interval of 2 ms from the inverse solution of q_w and T_w as shown in Fig.7 (a). The red dots indicate the boiling curve on the stagnation point plotted at the rotational period of 1 s.

In Fig.8(a) the locus of the boiling iterated loop in accordance with rotation of the cylinder and a loop was shifted from the higher wall superheat region to the lower superheat region. Noting change in the slope of the boiling curve denoted with the red dots, we can know the transient boiling heat transfer on the stagnation point is categorized into three regions: Single phase heat transfer (S.P.) region, Nucleate boiling (N.B.) region and Transition boiling (T.B) region. The single phase and nucleate boiling heat transfers indicated positive slope but the transition boiling was characterized with negative slope as shown in Fig.12. In the present experimental data, film boiling (F.B.) region could not be observed in the boiling curves. Even though the boiling situation was in "Non-wetted regime (a)" given in Figs.6 and 7 (a), partial and intermittent liquid-solid contacts on the stagnation point were implied from the result of Fig.8 (b). At earlier stage larger loop was drawn due in accordance with passing on the wet and dry areas, but after single phase heat transfer region included fully wetted situation denoted with $t_{wet,f}$, the boiling curve indicated monotonic change.
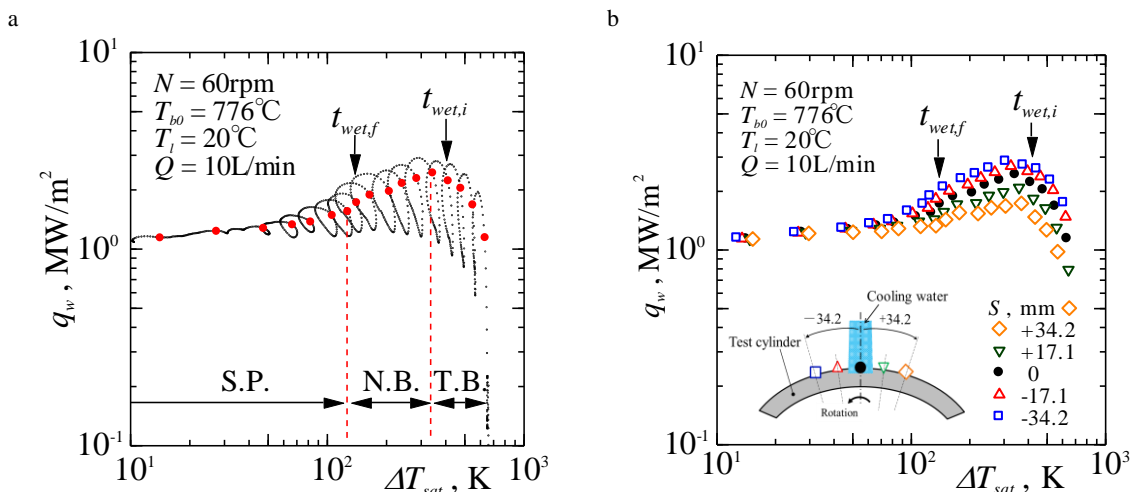
Fig.8 Boiling curve during rotating of cylinder. (a) locus of boiling curve (b) comparison of boing curves at circumferential positions

Figure 8(b) shows the boiling curves at different circumference positions which were 17 mm and 34 mm ahead or behind the stagnation point. The maximum heat flux of each boiling curve increased as the circumference position changed from $S = +34$ mm (behind the stagnation point) to S = -34 mm (ahead the stagnation point).

Figure 9 shows the comparisons of the boiling curves evaluated at the stagnation point for different laminar flow rate, degree of liquid subcooling, respectively. For reference, two correlations of single phase heat transfer coefficient in impinging jet cooling on the stagnation zone and film boiling heat transfer coefficient in subcooled jet impingement are given as Eqs.(1) and (2) by Liu, X. et al. [5] and Liu, Z.H. and Wang, J. [6]. These two correlations were derived by theoretical analysis for the stationary heated surface and steady state heat transfer.

In Fig.9(a) the boiling curve at $Q = 6$ and 10 L/min, indicates single phase convective heat transfer, nucleate boiling and transition boiling regions as denoted with S.P., N.B and T.B.. The S.P. and N.B. regions are distinguished by change in the slope of the boiling curve, and N.B. and T.B. regions are identified with maximal heat flux point and negative slope. The wall superheat recording the maximal heat flux was found to shift slightly to higher superheat side as increase in laminar flow rate. The boiling curves in transient laminar jet cooling indicates similar boiling curve with that in pool boiling but transient boiling curves shifted to much higher wall superheat.

The wall superheat at the maximum heat flux recorded about 300 K which is one digit higher than that of the pool boiling. As the laminar flow rate Q increased beyond 10 L/min, nucleate boiling region appeared to vanish, and the boiling curves indicating positive slope approached to the similar relationships given by Eq.(1). In case of maximum laminar flow rate of 23 L/min, transition boiling region did not come out in Fig. 12(b) as well as Fig. 12(a) and heat flux on the measured boiling curve was about 25 % lower than Eq. (1). Film boiling region which shows positive slope and exists at higher wall superheat beyond T.B. region as indicated by Eq.(2) was no appeared in the obtained boiling curves. Much higher initial wall superheat would be needed to obtain the film boiling region. In some boiling curves, the transition boiling region extended below the estimated film boiling curves estimated by Eq.(2).

In Fig.9(b), when the degree of subcooling ΔT_{sub} increased beyond 80 K, the transition boiling region shrank, namely it shifted to higher ΔT_{sub} region. According to the boiling curve shift to high wall superheat regime, ΔT_{sub} and Q have a similar effect. Under high ΔT_{sub} and Q conditions, characteristic of the heat transfer below the wall superheat

$$Nu_{d,o} = \begin{cases} 0.715\,\mathrm{Re}_d^{1/2}\,\mathrm{Pr}^{0.4} & 0.15 < \mathrm{Pr} < 3 \\ 0.797\,\mathrm{Re}_d^{1/2}\,\mathrm{Pr}^{1/3} & \mathrm{Pr} > 3 \end{cases} \qquad \text{Region1: Stagnation zone}(r/d<0.787) \qquad (1)$$

$$\mathrm{Nu}\left(=\frac{q_w d_j}{\Delta T_{sat}\lambda_l}\right) \approx 2\,\mathrm{Re}_l^{1/2}\,\mathrm{Pr}_l^{1/6}\left((\lambda_v/\lambda_l)(\Delta T_{sub}/\Delta T_{sat})\right)^{1/2} \qquad (2)$$
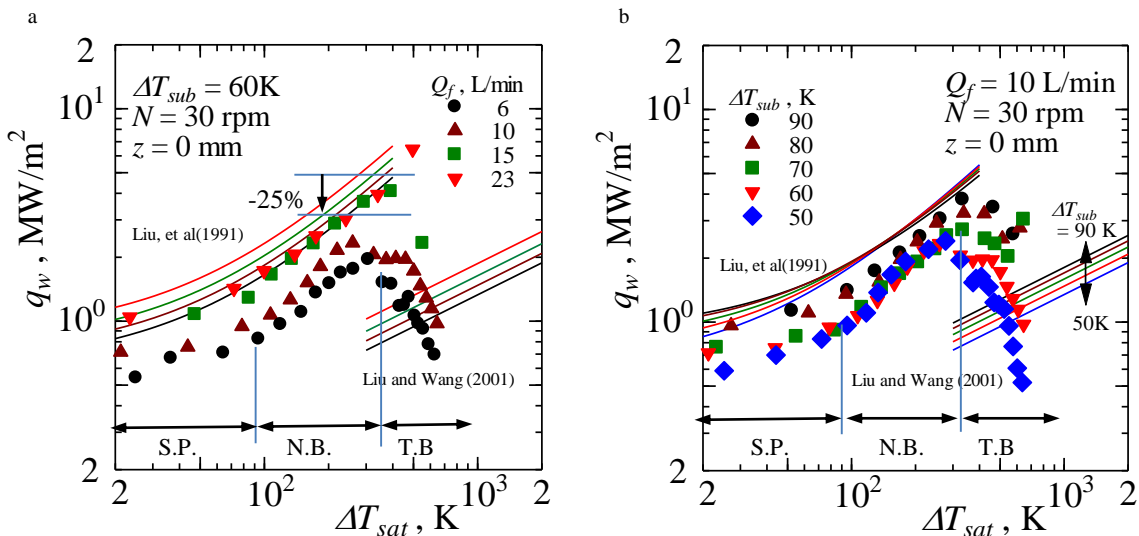
Fig.9 Comparison of boiling curves at the stagnation point; (a) effect of flow late, (b) effect of liquid subcooling

at the maximum heat flux point indicated very similar with the single phase convective heat transfer on the stagnation point. This fact also supported with the observation of the rewetting process shown in Figs.5 and 6.

4. Conclusions

The experimental study on the subcooled laminar jet quenching on the rotating hot hollow cylinder which simulates quenching of hot strips on the ROT has been done for extensive range of the flow rate, the jet temperature and the rotational speed. The highlights of the results are broadly concluded.

1. The propagation of the wetting area during the laminar jet quenching on the rotating hollow cylinder depended strongly on the moving direction of the hot surface. And the characteristic of the wetting area propagation with time was categorized into the four regimes based on change in distribution of wetting front in the circumferential direction.

2. The wetting temperature below which stable surface wetting situation could be seen on the stagnation area was very sensitive against the laminar jet temperature and the laminar flow rate.

3. The boiling curve on the stagnation area was divided into the boiling region being similar with steady state saturated pool boiling curve but it shifted for much higher wall superheat region. As the liquid subcooling and the laminar flow rate increased, the single phase convective heat transfer region dominated on the boiling curve and it was comparable with the existing theoretical correlation on the stagnation area of the impinging jet for steady state and stationary heated surface.

Acknowledgements

References

[1] Gradeck, M., Kouachi, A., Lebouché, M., Volle, F., Maillet, D., Borean, J.L., Boiling curves in relation to quenching of a high temperature moving surface with liquid jet impingement, Int. J. Heat and Mass Transfer, 52 (2009) 1094–1104
[2] Aloke Kumar Mozumderm, Mitsutake, Y. and Monde, M., Subcooled water jet quenching phenomena for a high temperature rotating cylinder, Int. J. of Heat and Mass Transfer, 68 (2014) 466–478.
[3] Arima, H., Monde, M. and Mitsutake, Y., Estimation of Surface Temperature and Heat Flux using Inverse Solution for One Dimensional Heat Conduction, Thermal Science and Engineering, 10 (2002) 27-37.
[4] Mitsutake, Y., Monde, M., Heat transfer during transient cooling of high temperature surface with an impinging jet, Heat and Mass Transfer, 37 (2001) 321-328.
[5] Liu, X., Lienhard, J. S. and Lombara, J. S., "Convective Heat Transfer by Impingement of Circular Liquid Jets", Trans. ASME Heat Transfer, 113 (1991) 571-582.
[6] Liu, Z.H, and Wang, J. ,"Study on film boiling heat transfer for water jet impinging on high temperature flat plate", Int. J. Heat and Mass Transfer, 40 (2001) 2475-2481.

6th BSME International Conference on Thermal Engineering (ICTE 2014)

Preparation of a Clamp Sleeve Spare Parts for Crimping Machine Using Low Carbon Steel Material by Heat Treatment Process

Md. Arefin Kowser[a], Muhammad Hurmutul Islam[b]

[a]*Associate Professor, Department of Mechanical Engineering, Dhaka University of Engineering and Technology, Gazipur,*
Country: Bangladesh
Email: nadimduet@yahoo.com
[b]*Post-Graduate student, Department of Mechanical Engineering, Dhaka University of Engineering and Technology, Gazipur*
Country: Bangladesh
Email: hurmutulislam@yahoo.com

Abstract

In Metered Dose Inhaler plant of pharmaceutical industries of Bangladesh, clamp sleeve spare part used in crimping machine collected from foreign countries. The clamp sleeve presses the crimping tong containing aluminium can to crimp the body with head. Due to the continuous action of the clamp sleeve to the crimping tong the inner surface of the clamp sleeve get corroded. The clamp sleeve is replaced when crimping appearance fails to meet compliance. In this Research an experimental work relating to improve the mechanical properties of locally available low carbon steel material by heat treatment process have been carried out to replace the spare parts of clamp sleeve which is collected from foreign countries. The mechanical properties have been studied on before and after heat treatment. After heat treatment, it is found that hardness, impact and compressive strength of heat treated specimen has been developed drastically as compared to that of before heat treatment. Finally, the properties of improved material has been determined and used to the machine functional area to check the performance of the clamp sleeve. After consecutive operation of the machine it can be concluded that the improved clamp sleeve meets the user requirement with compliance of smooth crimping quality and locally available low carbon steel material can be used for the preparation of clamp sleeve spare parts of crimping machine for pharmaceutical industry using the proper heat treatment process which might be helpful to save huge cost and time rather than collected from foreign countries.

* Corresponding author. Tel.: +8801754262832; fax: +88029204710.
E-mail address: nadimduet@yahoo.com

1. Introduction

As a developing country Bangladesh is not taking any initiative to manufacture any equipment even not intend to develop the preparation of spare parts of the equipment in industrial application. The use of low carbon steel is one of the solutions for reducing cost in industrial applications. So, in this research the focus is to locally develop a clamp sleeve spare part for crimping machine of Metered Dose Inhaler (MDI) plant of pharmaceuticals application using locally available low carbon steel material by heat treatment process. Carburizing is the addition of carbon to the surface of low-carbon steels at temperatures within the austenitic region of the steel concern, which generally is between 850°C and 950°C. Within this temperature range austenite has high solubility for carbon and is the stable crystal structure. Babu and Bhadeshia [1] modeled carbon diffusivity in accordance with kinetic and thermodynamic behavior of carbon in austenite. The study of process parameters in metals during heat treatment has been of considerable interest for some years [2-5] but there has been relatively little work on process variables during the surface hardening process [6] since controlling parameters in carburization is a complex problem. The major influencing parameters in carburization are the holding time, carburizing temperature, carbon potential and the quench time [7]. The aim of research work is to improve the mechanical properties of low carbon steel applicable for pharmaceuticals industries. In MDI plant, there is a crimping machine which purpose is to crimp the body of the aluminium can with head. The major part of the crimping machine is the crimping head. Inside crimping head, there are clamp sleeve and crimping tong. The clamp sleeve press the crimping tong to crimp the aluminium can through the up and down movement of the piston shaft by air pressure with the application of pneumatic control valves and the aluminium can after smooth crimping is released through the up and down movement of the main piston shaft by air pressure with the application of pneumatic control valves.The Clamp Sleeve has been made using low carbon steel which is cheap, locally available but it has less hardness. So, the purpose of the research work is to improve hardness of locally developed clamp sleeve through the heat treatment process and to implement it to the machine functional area to meet the same purpose as it done earlier using the foreign clamp sleeve part.The crimping machine and the clamp sleeve part is shown in Fig. 1 and in Fig. 2.
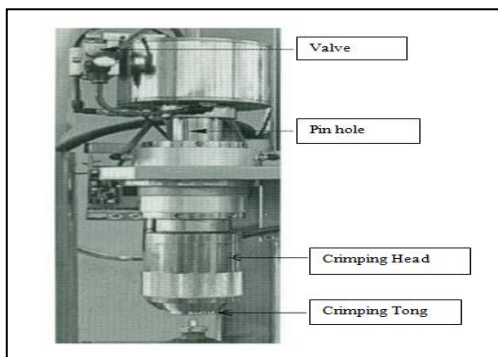
Fig. 1. Crimping machine.

Fig. 2. Clamp sleeve spare part of crimping machine.

The Physical and Mechanical properties of low carbon steel are shown in Table 1 and Table 2, respectively.

Table 1. Physical properties of locally available material[8].

Parameter	Range
Density	7.86 Kgm^{-3}
Thermal Expansion(10^{-6} k^{-1})	11.7
Thermal Conductivity	50 J/m ks
Young's Modulus	210 GPa
% Elongation	30

Table 2. Mechanical properties of locally available material [8].

Parameter	Range
Hardness , Brinell/Rockwell B	126/71
Tensile strength ,Ultimate /Yield	440 MPa /370 MPa
Poisson's ratio	0.29
Shear Modulus	80.0 GPa

Nomenclature

ASTM	American Society for Testing and Materials
BHN	Brinell Hardness Number
HRC	Rockwell Hardness
MDI	Metered Dose Inhaler
UTM	Universal Testing Machine
ε_E	Engineering Strain
ε_T	True Strain
σ_E	Engineering Stress
σ_T	True Stress
l_0	Initial length
l_f	Final length

---

2. Experimental

2.1 Specimen Preparation

Low carbon steel solid round bar is purchased from a reliable local source. The material is then machined and finished as per sample. Physical dimension of different test Specimen is shown in Table 3.

Table 3. Physical dimensions of different test specimen.

Sl. No.	Name of Test	Dimension of the Specimen								
					V notch		Grip		Gauge	
		Length (mm)	Width (mm)	Thickness (mm)	Depth (mm)	Included Angle	Distance (mm)	Dia. (mm)	Length (mm)	Dia. (mm)
1	Hardness	58	9.3	9.3	-	-	-	-	-	-
2	Impact	58	9.3	9.3	6.6	60°	-	-	-	-
3	compression	-	-	-	-	-	35	18	20	10

2.2 Heat Treatment of Materials

Low Carbon Steel is primarily heat treated to create matrix microstructures and associated mechanical properties. The principle objective of this research is to carry out heat treatment of prepared clamp sleeve (material: low carbon steel) and to compare the mechanical properties of before and after heat treatment of locally purchased low carbon steel material. In Pack carburizing the specimen was heated to a temperature of 900°C for 6 hours to achieve case depth 3 mm. of deposition with respect to time and temperature is shown in Table 4.

Table 4. Case depth of deposition with respect to time and temperature [9].

Time (Hr) at Temp.°C	Case depth in mm				
	700°C	900°C	925°C	950°C	980°C
1	0.45	0.55	0.65	0.75	0.85
2	0.55	0.75	0.9	1.05	1.2
3	0.65	0.95	1.1	1.3	1.5
4	0.75	1.1	1.25	1.5	1.75
5	0.85	1.2	1.4	1.7	1.95
6	1.1	1.3	1.55	1.85	2.15
8	1.25	1.5	1.8	2.1	2.45
10	1.4	1.7	2.0	2.35	2.75

After the operation, the furnace is switched off due to the temperature of the specimen will decrease with the same rate as that of the furnace. The specimen has been taken out of the furnace when the furnace temperature had already reached to room temperature. In quenching the specimen is heated to a temperature of 850°C for 15 minutes to homogenize the specimen at that temperature. After 15 minutes, the specimen was taken out from the furnace and directly quenched by rapid cooling using the quenching medium as water solution of 10 percent sodium chloride called brine Solution. In tempering, the specimens was heated to 150°C for 1 hour to reduce the tendency for internal stress formation. After heat treatment, the specimen is air cooled by normal air. Time Vs Tempering Temperature curve is shown in Fig. 3.
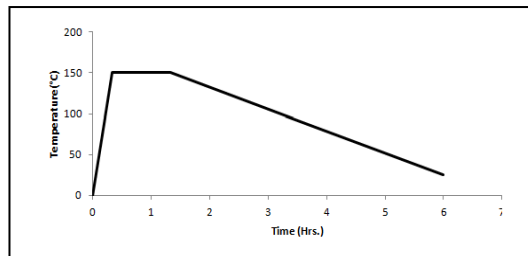
Fig. 3. Time-Temperature curve of tempering process.

3. Test Parameter

3.1 Hardness Measurement

Before heat treatment the hardness of the specimen is measured by Brinell hardness tester but due to improvement of hardness after heat treatment, hardness measured by Rockwell hardness tester. After heat treatment, the hardness of the specimen has increased where the reading might exceed the maximum limit of the dial gauge of Brinell hardness tester. So, the Brinell hardness tester is preferred for hardness test of material before heat treatment and Rockwell hardness tester is preferred for hardness test of material after heat treatment. The hardness is obtained in HRC. Equation (1) is used to convert values:

$$BHN = 17.515 \times HRC \qquad \text{(When the HRC Values51-60)} \qquad (1)$$

Using the conversion Table, BHN value was converted into Rockwell hardness HRC value. Heat treated specimen was measured in HRC means Rock well Hardness C Scale which is suitable to measure hardness of hard material.. Hardness test results of specimen before and after heat treatment are presented in Fig. 4.
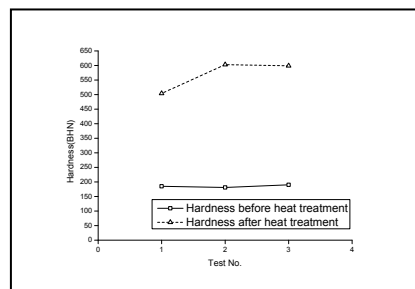
Fig. 4. Hardness of specimen before and after heat treatment process.

From the Hardness test results it can be observed that the average hardness has been increased about three times.

3.2 Impact Strength Measurement

These tests have been conducted for before and after heat treated specimen using three samples in each test. The test consists of measuring the energy absorbed in breaking a V– notched specimen by giving a single blow by swinging hammer. The specimen is simply supported at its ends. As the velocity of striking body is changed, there must occur a transfer of energy. It is usually measured by the energy absorbed in a notched impact test like charpy or izod tests. The working condition of charpy tester used for Impact test is presented in Table 5.

Table 5. Working conditions of GAMCO charpy tester.

Parameter	Range
Weight of Hammer	10 Kg
Striking of Hammer	4 cm/s to 5 cm/s
Angle of hammer striking edge	30°
Radius of curvature of striking edge	2 mm
Swing of hammer both ways	0-160°

Figure 5 shows the impact test results of specimen before and after heat treatment. From impact test results it can be observed that the average energy absorption rate has been increased about two times after heat treatment than that of before heat treatment.
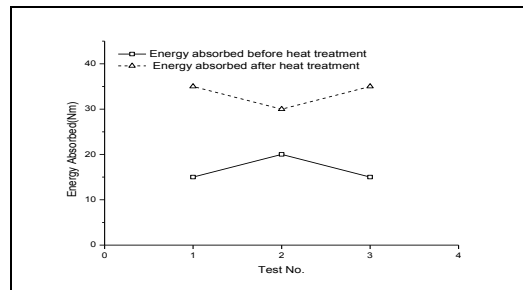
Fig. 5. Impact strength of specimen before and after heat treatment.

3.3 Compressive Strength Measurement

The compressive strength is measured by compression test using universal testing machine (UTM) before and after heat treatment. The parameters were considered during compression test is shown in Table 6. Engineering Stress is converted to true stress using equation (2). Engineering strain is converted to true strain using equation (3).

$$\sigma_T = \sigma_E(1 + \varepsilon_E) \tag{2}$$

$$\varepsilon_T = \ln(1 + \varepsilon_E) \tag{3}$$

Table 6. Experimental condition during compression test by universal testing machine.

Parameter	Experimental condition
Cross head Speed (mm/min)	0.05
Loading Range(KN)	0-50
Humidity (%)	70%
Temperature (°C)	24°C

a)   b)   c)
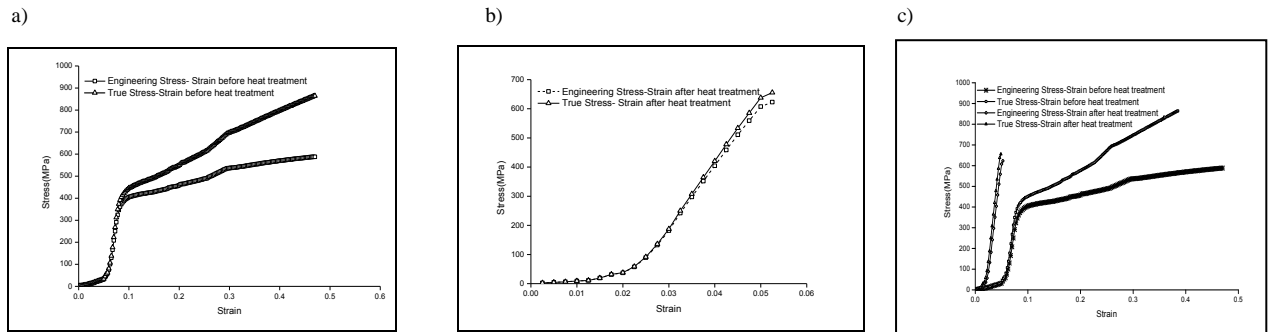
Fig. 6. Engineering and true stress strain diagram of compression test (a) before heat treatment; (b) after heat treatment; (c) Combined curve.

From the Combined curve it is shown that for a fixed strain of 0.03, before and after heat treatment the stress was at about 10 MPa and 200MPa, respectively .From the diagram it can also be concluded that after heat treatment of the specimen the strength of the material has been developed. Due to maximum load capacity in our lab is 50 KN, it is possible to apply load up to maximum capacity that's why after heat treatment material could not apply load up to breaking point. Results of compression test are shown in Table 7.

Table 7. Compression test results before and after heat treatment.

Test No.	Before Heat treatment		After Heat treatment	
	Applied Load (N)	Specimen Condition	Applied Load (N)	Specimen Condition
1	46150	Deformed	48900	Non-Deformed
2	46200	Deformed	48850	Non-Deformed
3	46300	Deformed	48850	Non-Deformed

3.4   Material Composition Study

Chemical composition of low carbon steel material before and after heat treatment is presented in Table 8.

Table 8. Chemical composition of specimen before and after heat treatment by optical emission spectrometer.

Sl. No.	Name of the Ingredients	Chemical Composition (weight %)	
		Before Heat Treatment	After Heat Treatment
1	Iron (Fe)	99.220	98.854
2	Carbon (C)	0.13942	0.68420
3	Silicon(Si)	0.00000	0.00000
4	Manganese(Mn)	0.46210	0.32305
5	Phosphorous(P)	0.01757	0.01608
6	Sulphur(S)	0.01770	0.01252
7	Copper(Cu)	0.12902	0.09650
8	Chromium(Cr)	0.01357	0.01265
9	Boron(B)	0.00082	0.00075

It seems that the % of C is increased almost five times after heat treatment than that of before heat treatment which indicates the sign of improvement of hardness. A comparison of key elements is presented in Table 9.

Table 9. Comparison of improved local material with foreign material.

Test No.	Key Elements	Clamp Sleeve (Locally Prepared)	Clamp Sleeve (Collected from foreign countries)
1	Durability	Durable.	Durable
2	Quality	Meets requirement.	Meets requirement
3	Availability	Available whenever required	Not possible to provide any time due to foreign parts
4	Stock Maintenance	Does not require as it is easily available.	Requires to keep a lot in stock as
5	Price	Comparatively less	Comparatively high

4. Cost Savings

Currently in MDI Plant, Semi Automatic and Automatic crimping machine are used approx. twenty renowned Pharmaceuticals companies in Bangladesh. The total expenses for purchasing consumable spare items from foreign countries are approx. 57, 60,000 BDT. Whereas making locally for semi automatic crimping machine the unit cost will bring 2,300 BDT. And for automatic crimping machine the unit cost will bring 2,900 BDT. The total expenses are approx. 12, 78,000 BDT. Which means the possibility to save expenses per year is approx. 44, 82,000 BDT.

5. Conclusion

In this Research an experimental work relating to improve the mechanical properties of locally available low carbon steel have been carried out to replace the spare parts of clamp sleeve of crimping machine collected from foreign countries using the heat treatment process. The mechanical properties have been studied on before and after heat treatment of specimen. Three individual samples have been chosen and the average values of the three specimens for each test have been presented. From this experiment it is found that hardness, impact and compressive strength of heat treated specimen has been developed drastically as compared to the specimen before heat treatment. Finally, the properties of improved material has been determined and used to the machine functional area to check the performance of prepared clamp sleeve. After consecutive operation of the machine it can be concluded that the improved clamp sleeve meets the user requirement with compliance of smooth crimping quality and locally available low carbon steel material can be used for the preparation of clamp sleeve spare parts of crimping machine in pharmaceutical industry using the proper heat treatment process which might be helpful to save huge amount of cost and time rather than collected from foreign countries.

References

[1] S.S Babu, H.K.D.H. Bhadeshia, Diffusion of Carbon in Substitutionally Alloyed Austenite, Journal of Materials Science Letters, 14(5), 1995, pp. 314-316.
[2] S. Denis, Coupled temperature stress, phase transformation calculation model numerical illustration of the internal stresses evolution during cooling of a eutectoid carbon steel cylinder, Metallurgical Transaction A,18A, 1987, pp. 1203-1287.
[3] J.B.Leblond, Mathematical modeling of transformation plasticity in steels I: Case of ideal plastic phases II: Coupling with strain hardening phenomena, International Journal of Plasticity, 5, 1989, pp. 551-591.
[4] K.F.Wang, S.Chandrasekar, H.T.YYang, Experimental and computational study of the quenching of carbon steel, International Journal of Manufacturing Science and Engineering, 119, 1997, pp. 257-265.
[5] C.C. Liu, X.J. Xu, Z. Liu, A FEM modeling of quenching and tempering and its application in industrial engineering, International Journal of Finite Elements in Analysis and Design,39, 2003, pp.1053-1070.
[6] G.P.Shewmon, Diffusion in solids, series in material science and Engineering, Mc Graw Hill, Tokyo, 1963.
[7] R.Hochman, J.Burson, The Fundamentals of Metal Dusting,NewYork: API Division of Refining, 46, 1966, p.331.
[8] V.Raghavan, Material Science and Engineering, 4thEdition, Prentice Hall of India Ltd., 1994, pp. 396.
[9] P. E. Home,"case depth: an attempt at practical diffusion", MP, 1943, pp. 265-272.